applied sciences

MDPI

Article

Reliability Optimization Design of Constrained Metamorphic Mechanism Based on the Augmented Assur Groups

Qiang Yang [1,2,*], Hongxiang Zhang [1,*], Benqi Sun [1], Yuan Gao [1] and Xin Zhao [2]

[1] College of Mechanical Engineering and Automation, Northeastern University, Shenyang 110819, China; zhx89596038@163.com (B.S.); 2370122@stu.neu.edu.cn (Y.G.)
[2] Key Laboratory of Lifting Equipment's Safety Technology for State Market Regulation, Shenyang 110004, China; zxvir@163.com
* Correspondence: qiangyang@mail.neu.edu.cn (Q.Y.); 2200462@stu.neu.edu.cn (H.Z.)

Abstract: In order to obtain stable and reliable configuration transformation ability, reliability optimization design is regarded as an effective way to reduce the probability of kinematic function failure for the constrained metamorphic mechanism. Based on the structural composition principle of multi-configuration source metamorphic mechanism that can operate in an under-actuated state, the modularized calculation methods are established for the force analysis of augmented Assur groups including metamorphic kinematic joints. According to the equivalent resistance gradient model of metamorphic mechanisms, with considering the uncertainties in the link dimensions, masses, and compliance parameters et al., a probabilistic evaluation method for describing the configuration transformation ability of the constrained metamorphic mechanism is established. Based on reliability evaluation and reliability sensitivity analysis, a reliability optimization design method for improving the configuration transformation ability is proposed, and then the optimization design is carried out for tolerances of random variables focusing on those structural parameters with higher reliability sensitivity, so that the optimized results can satisfy the requirements of both reliability and economic simultaneously. Finally, the feasibility and effectiveness of the proposed method is verified by the illustration of a paper folding metamorphic mechanism. The research provides the foundation of reliability design of metamorphic mechanisms to obtain the high-probability repeated execution ability of configuration transformation, it also has theoretical and practical significance to promote the engineering application of metamorphic mechanisms.

Keywords: constrained metamorphic mechanisms; reliability optimization design; configuration transformation; optimal design; reliability sensitivity; metamorphic kinematic joints

Citation: Yang, Q.; Zhang, H.; Sun, B.; Gao, Y.; Zhao, X. Reliability Optimization Design of Constrained Metamorphic Mechanism Based on the Augmented Assur Groups. *Appl. Sci.* **2024**, *14*, 6524. https://doi.org/10.3390/app14156524

Academic Editor: Jérôme Morio

Received: 14 June 2024
Revised: 16 July 2024
Accepted: 23 July 2024
Published: 26 July 2024

1. Introduction

At the 25th ASME Annual Conference on Mechanism and Robotics in 1998, Dai et al. [1] first proposed the concept of metamorphic mechanisms. The mechanism has the ability of self-reconfiguration according to different task requirements and working conditions, which has attracted significant interest all over the world. Jin et al. [2] established a dynamic analysis model of the metamorphic mechanism by using the Kane equation. Dai et al. [3] systematically expounded the principle of mesomorph and a general categorization of metamorphic mechanisms. Guo et al. [4] studied the topological analysis of variable mobility mechanisms by applying the metamorphic principles. Lan et al. [5] put forward a new adjacency matrix to describe the topological changes of metamorphic mechanisms, which can not only preserve the information of the original mechanism but also derive all possible changes of the mechanism. Li et al. [6,7] presented the structure composition principle of single-driven metamorphic mechanisms based on augmented Assur groups, and then defined a non-dimension equivalent resistance coefficient of metamorphic joints and an equivalent resistance gradient model of metamorphic mechanisms. Kanner et al. [8]

studied the influence of variations in design parameters on the passive adaptability of underactuated robot legs to uneven terrain and discussed the stability of the robot with respect to their postures. Coppola et al. [9] proposed a methodology named re-configurable dynamics to reconfigure the kinematics and dynamics parameters. Wang et al. [10] established a nonlinear dynamic model of a novel metamorphic palletizing robot to describe all the configurations under actual operating when its configuration changed from 1-DOF to 2-DOF. Yang et al. [11] studied the types of synthesis of constrained metamorphic mechanisms with structural forms of metamorphic joints. Li et al. [12] first proposed a new method for analyzing the constraint force of metamorphic kinematic joints, which provided the basis for dynamic analysis of metamorphic mechanisms. Wang et al. [13] carried out static analysis of an underactuated manipulator, analyzed its grasping stability and optimized its structural parameters. Aimedee et al. [14] addressed metamorphic and reconfigurable mechanisms based on types of morphing and ways of achieving it considering various types of morphing, mainly including topological morphing [15,16], geometrical morphing [17,18] and furcating morphing [19,20], etc. Tian et al. [21] introduced a method for configuration synthesis of metamorphic mechanisms on the basis of five metamorphic modes: the geometry, motion, force, driving joint and combined metamorphic mode. Qiao et al. [22] calculated the general static contact force of a 3-DOF underactuated robotic finger using the principle of virtual work and analyzed its self-adaptive grasp process and equilibrium configuration. Song et al. [23] built a unified dynamics model of constrained metamorphic mechanisms. Based on the model, the kinematic laws of all components, the driving force/torque of the driving link and the constraint force/torque of the metamorphic joints can be obtained. Yang et al. [24] proposed a general structural design method for a planar metamorphic mechanisms based on the structural synthesis matrix. Liu et al. [25] established a full-configuration kinematic reliability model of a planar five-bar metamorphic mechanism considering multi-source uncertainties such as joint clearances, manufacturing tolerances of links, thermal deformations of links and joints.

Reliability optimization design is one of the important branches of reliability design. There are mainly two ideas about how to optimize: (1) Maximize reliability of the mechanism when it meets the requirements of performance and/or cost; (2) Minimize factors of the mechanism such as cost, volume and weight, under the condition of meeting the reliability requirements. With the development of computer technology and programming, more and more advanced optimization algorithms are applied to reliability optimization. Liao et al. [26] employed genetic algorithm to complete the error optimization of a new 6-DOF parallel mechanism, which provided foundation for the research on tolerance optimization. Pan [27,28] used self-adaptive genetic algorithm and fuzzy genetic algorithm to optimize the cost–tolerance model of a 6-DOF parallel robot. Chen et al. [29,30] analyzed the kinematics performance of 4-UPS-RPU parallel mechanism and optimized its structure parameters based on the global dexterity coefficient. Ni et al. [31] transformed the design of tolerances into a nonlinear optimization design with constraints based on sensitivity analysis and applied genetic algorithm to distribute the manufacturing tolerances of a parallel machine tool finally. Xiong [32] applied fuzzy theory to the multi-objective optimization design of a double-stage wheel hub reducer system taking the minimum volume and maximum reliability as the objective function.

Kang and Dai [33] pointed out that: "It is of great significance for the innovation and development of advanced manufacturing technology and a new generation of robots to study intelligent reconfigurable mechanisms and robots with the ability to actively adapt to changing environments and working conditions and passively adapt to emergencies". The ability of convenient variable-working configuration/variable-topological structure is an important performance of metamorphic mechanism. The precise transforming of adjacent configurations and the maintenance of each working configuration are the basis for metamorphic mechanism to complete the operational tasks. At present, some researchers [34] have point out that: "It has always been an unsolved problem to switch their motion patterns smoothly and reliably for multi-mode mechanisms/multiconfiguration mecha-

nisms". Although through years of unremitting efforts by scholars around the world, the basic theoretical research on metamorphic mechanisms has become increasingly rich, the engineering application research is also gradually being carried out [35,36]. Due to the "unresolved problem" proposed in reference [34], the engineering application of metamorphic mechanisms is not very ideal. At present, the reliability of configuration switching in metamorphic mechanisms has not received sufficient attention from scholars all over the word. Chang et al. [37] established an impact force calculation model for metamorphic mechanism during the process of configuration switching based on contact collision theory. Reference [38] established the dynamic model of a planar five-bar metamorphic mechanism using Lagrange equation and solved the impact and vibration during the configuration transforming. Reference [39] completed the dynamic simulation during configuration transforming of a metamorphic lifting mechanism using ADAMS 2019 software (version number: 29.0.0). However, the above research in reference [37–39] does not involve probability issues and cannot reveal the randomness of kinematic failure of configuration transformation. References [40–42] attempt to conduct randomness analysis of configuration transformation for metamorphic mechanisms, but the authors' research all focuses on solving the equivalent resistance coefficient of metamorphic joints and does not solve the problem of calculating the probability of kinematic failure during the configuration transformation.

In recent years, some scholars have paid attention to the reliability of configuration maintaining of metamorphic mechanisms and made corresponding research progress. Liu et al. [25] established a full-configuration kinematic reliability model of a planar five-bar metamorphic mechanism considering multi-source uncertainties such as joint clearances, manufacturing tolerances of links, thermal deformations of links and joints. In references [43,44], Wang et al. considered the influence of internal impact during configuration transformation, taking a controllable metamorphic palletizing robot as the research object, considering the multiple failure modes and the random and interval variables, and proposed a vibration reliability evaluation method during the configuration maintenance period after configuration transforming. However, the studies in references [43,44] have focused more on the kinematic or dynamic reliability analysis of metamorphic mechanisms within each configuration maintaining period. Obviously, compared to configuration maintenance, the kinematic failure of switching between adjacent configurations is a more likely failure model for metamorphic mechanisms. Therefore, conducting reliability research on configuration switching has more theoretical and practical significance. Particularly for constrained metamorphic mechanisms, the transforming/maintenance of working configurations is mainly realized by the transforming/maintenance of the moving and static of the metamorphic kinematic joints (variable kinematic joints). Therefore, some specific "switching" structures of metamorphic joints need to be designed for realizing the transformation between moving and static. The inborn attribute of metamorphic joint determines that the failure of configuration transformation is the most frequent failure mode for the constrained metamorphic mechanism in completing operational tasks, and the ability of completing configuration transformation precisely is a crucial indicator for performance of the metamorphic mechanisms. Obviously, the reliability-based optimization design focusing on the stability of configuration transformation is the basis of improving the stability and reliability of configuration transformation. Currently, little literature is introduced about systematical research on the probability evaluation and the reliability-based optimization design of configuration transformation ability based on the force analysis during the kinematic status switch of metamorphic joints at the moment of configuration transformation. Based on the equivalent resistance gradient model, the study aims to establish a probability evaluation model of the configuration transformation ability of the constrained metamorphic mechanism, and propose a reliability optimization design method aiming at obtaining a high probability of repeated implementation ability of configuration transformation, which provides a theoretical basis and an effective design basis for promoting the engineering application of constrained metamorphic mechanisms. The remainder of the paper is organized as follows: Section 2 introduces the working process

and structure composition principle of constrained metamorphic mechanisms. Section 3 proposes modularized force analysis methods of constrained metamorphic mechanisms first and then completes the structural design for a novel metamorphic revolute joint according to force analysis. Section 4 establishes the evaluation model of configuration transformation ability of constrained metamorphic mechanism under deterministic parameters and then presents a probabilistic evaluation model of configuration transformation ability by considering the randomness of input errors in practical application. Section 5 proposes a reliability-based optimization design method of constrained metamorphic mechanisms oriented to the stability of configuration transformation. In Section 6, the proposed method of reliability optimization design is illustrated by an example of the paper folding metamorphic mechanism to verify its feasibility and effectiveness. Finally, a discussion is presented in Section 7, and Section 8 concludes the paper.

2. General Metamorphic Working Process and Structure Composition Principle of Constrained Metamorphic Mechanisms

2.1. General Working Process of Constrained Metamorphic Mechanisms

A general metamorphic working process of the constrained metamorphic mechanism is as following: by transforming the moving/static kinematic status of metamorphic joints based on geometric constraints and/or force constraints provided by the specific structures of the links and joints, the multi-DOF source metamorphic mechanism is degenerated into a single-DOF metamorphic mechanism to form the corresponding working stages and keep the working configuration of the mechanism for completing the desired operational task. Then, by releasing the constrained metamorphic joint and constraining other metamorphic joints, the working configuration is transformed and another working stage is formed. Another operational task is accomplished by keeping the working configuration. The working sequences of required working stages are controlled by constraining different metamorphic joints in the sequences. To obtain all the working configurations of metamorphic mechanism, all the metamorphic kinematic joints should be constrained alternately according to the required working stages and working sequences. Figure 1 is a 2-DOF constrained metamorphic mechanism with a single driver, and Figure 2 is the metamorphic cyclogram of the mechanism which describes the change in kinematic status of kinematic joints with different configurations. As can be seen from Figures 1 and 2, the constrained metamorphic mechanism in Figure 1 realizes two working configurations/topological structures of crank–slider mechanism and crank–rocker mechanism by using the kinematic status transformations of metamorphic joints R_3 with combined constraints of spring force and geometric constraints and P_7 with geometric constraints, as shown in Figure 2 (R represents revolute joint and P represents prismatic joint), and then completes the corresponding operational tasks in their respective working configurations.

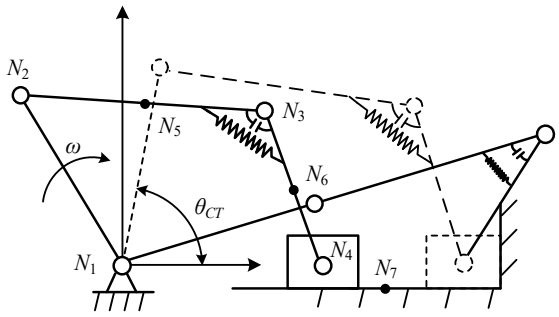

Figure 1. 2-DOF constrained metamorphic mechanism.

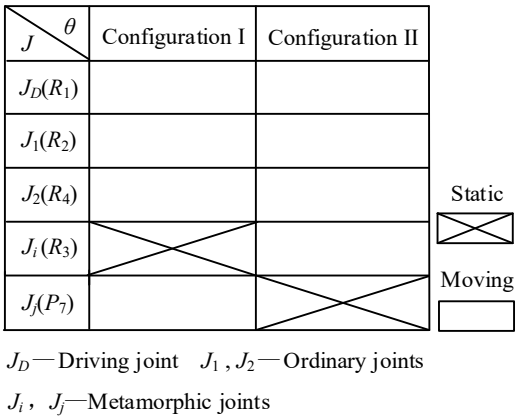

Figure 2. Metamorphic cyclogram of the 2-DOF constrained metamorphic mechanism.

2.2. Structure Composition Principle of Constrained Metamorphic Mechanisms

According to the structure composition theory of traditional mechanisms [45], any planar mechanisms can be formed by means of adding several elements of the Assur groups (AGs) to the driver link and the frame and/or the former element of the AGs and the frame [46,47]. The class II Assur groups are widely applied in the planar mechanisms, which are divided into five different elements. If an additional binary link and a revolute joint or prismatic joint are added into any element of the five class II AG elements, The DOF of the new element in the augmented groups is one instead of zero in the class II AG, and the augmented groups are named the class II Augmented Assur groups (AAGs) [7], which have nine different forms, as shown in Figure 3a–i.

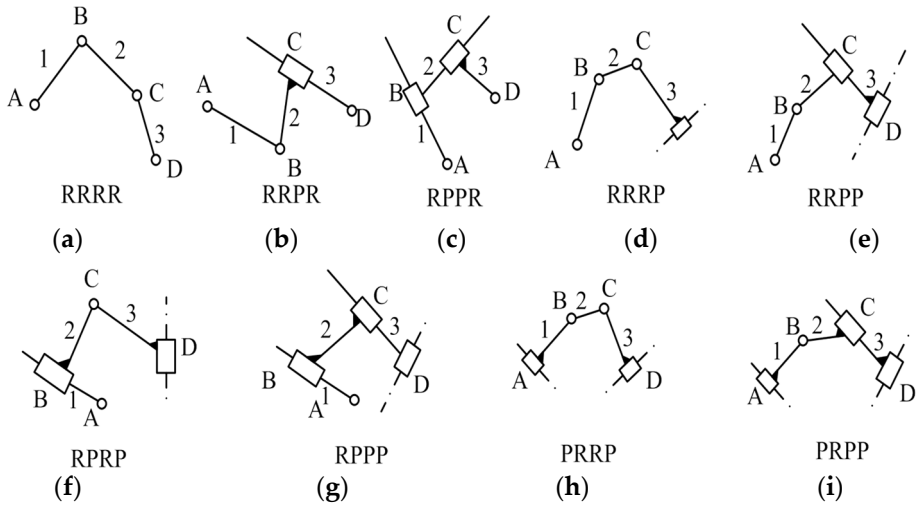

Figure 3. Nine structural forms of class II augmented Assur group.

In order to obtain an n-DOF constrained metamorphic mechanism operated by a single actuator, a convenient way is to make $n-1$ metamorphic joints static to eliminate $(n-1)$-DOF during every working stage. According to the idea, a structure composition principle of the n-DOF source mechanism based on the augmented Assur groups can be described as follows.

$$n\text{-DOF source mechanism} = (1\text{-DOF driver}) + (n-1) \times (1\text{-DOF group}) + x\ (0\text{-DOF group}) \quad (1)$$

As shown in Equation (1), x represents an arbitrary integer which is equal to or greater than zero. Based on 1-DOF augmented Assur groups summarized in Figure 3, $n-1$ of these 1-DOF AAGs and any 0-DOF AGs are connected to the 1-DOF driving link, frame, or ahead AAGs/AGs in sequence, which compose one of the n-DOF source mechanisms

shown in Equation (1). Therefore, the 2-DOF constrained metamorphic mechanism as shown in Figure 1 can be regarded as a 1-DOF augmented Assur group (RRRP shown in Figure 3d) connected to the driving link and the frame in sequence.

For an *n*-DOF source mechanism, according to the structure composition principle described in Equation (1) and Figure 1, *n* metamorphic joints must be arranged into it to obtain *n* working configurations. For the *n* metamorphic joints of the *n*-DOF source mechanism in the case of one driving link, only one metamorphic joint keeps moving in each working stage while the others remain static. Therefore, in order to realize all working configurations, every metamorphic joint must be constrained in sequence according to the required working stages according to Figure 2. Obviously, the kinematic status of the metamorphic joint depends on the driving force/torque and constraint force/torque acted on it.

3. Modularized Force Analysis of Constrained Metamorphic Mechanisms and Structural Design of Metamorphic Revolute Joints

According to structure composition principle of constrained metamorphic mechanisms based on augmented Assur groups, taking the driving link, AGs and AAGs as the basic units, the mathematical relationships between the kinematic or force analysis of each unit are deduced. In the paper, kinematic and force analysis of AAGs can be completed on the basis of the general kinematic and force analysis approach of the class II AGs.

Since every metamorphic joint must be constrained in sequence according to the required working stages, take one AAG as an example, one of the metamorphic joints can be constrained in the corresponding configuration of the metamorphic process, and the AAG can degenerate into the corresponding equivalent AG. Therefore, the kinematic and force analysis of the AAG can be carried out in different working configurations, and which are equal to the analyses of the corresponding equivalent Assur group in each working configuration. Since the kinematic analysis method of the augmented Assur group [48] is nearly the same as that of the corresponding Assur group, the paper builds the calculation model of force analysis of the augmented Assur group containing metamorphic joints based on the general force analysis of the Assur group. Because modularized force analysis of the nine elements of augmented Assur groups is similar to each other, the AAG RRRP included in the metamorphic mechanism shown in Figure 1 is taken as an example to illustrate the procedure of analysis.

In different working configurations, the equivalent Assur group of the AAG RRRP is shown in Figure 4, where the revolute joint 2 and the prismatic joint 4 are metamorphic joints. In working configuration I, link 1 and link 2 are annexed into a united one because metamorphic revolute joint 2 is constrained to keep static, and metamorphic prismatic joint 4 moves simultaneously, so the AAG RRRP degenerates into the RRP group. In working configuration II, the metamorphic prismatic joint 4 is constrained to transform from moving to static, the metamorphic revolute joint 2 changes from static to moving, so the AAG RRRP degenerates into the RRR group. The derivation process of modularized force analysis of the AAG RRRP is given as follows.

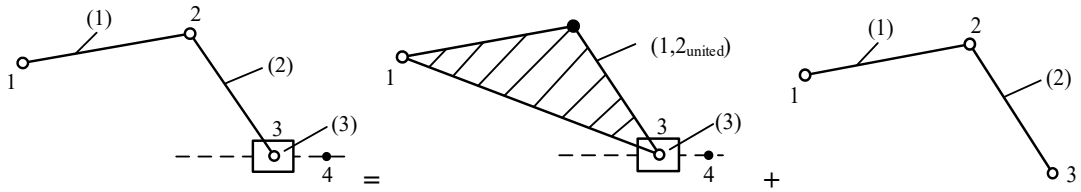

(**a**) Augmented Assur group RRRP (**b**) Configuration I (**c**) Configuration II

Figure 4. Metamorphic process of RRRP group.

3.1. Modularized Force Analysis of AGGs

In working configuration I, the AAG RRRP degenerates into the Assur group RRP. The force analysis of the corresponding equivalent Assur group RRP is shown in Figure 5,

where points N_5, N_6 and N_7 are the centroids of the links N_2N_3, N_3N_4 and the slider, respectively, and F_β is the component of the external force acting on the slide along the moving direction. Supposing that the external forces F_5, F_6, F_7 and torques T_1, T_2, T_3 acting on the links N_2N_3, N_3N_4 and the slider, respectively, are known, the reaction force of each revolute joint and the driving torque and constraint torque of the metamorphic revolute joint are solved.

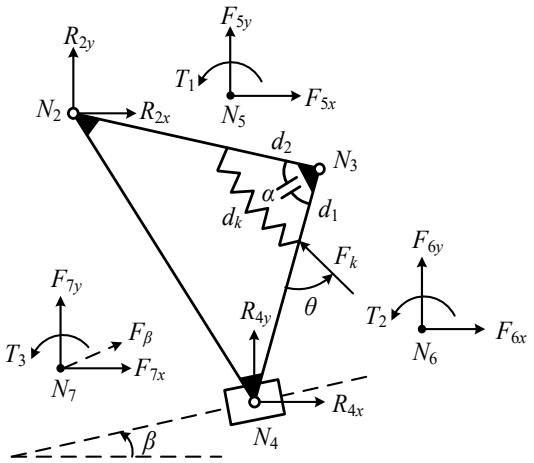

Figure 5. Force diagram of RRP group degraded by RRRP group.

Modularized force analysis procedures are as follows:

$$\cos\alpha = \frac{l_{23}^2 + l_{34}^2 - l_{24}^2}{2l_{23}l_{34}} = \frac{d_1^2 + d_2^2 - d_k^2}{2d_1d_2} \tag{2}$$

$$d_k = \sqrt{d_1^2 + d_2^2 - \frac{d_1d_2\left(l_{23}^2 + l_{34}^2 - l_{24}^2\right)}{l_{23}l_{34}}} \tag{3}$$

$$F_k = k(a - d_k) \tag{4}$$

$$\cos\theta = \frac{d_k^2 + d_1^2 - d_2^2}{2d_kd_1} \tag{5}$$

$$\theta = \arccos\left[\frac{2d_1^2 - \frac{d_1d_2\left(l_{23}^2+l_{34}^2-l_{24}^2\right)}{l_{23}l_{34}}}{2\sqrt{d_1^2 + d_2^2 - \frac{d_1d_2\left(l_{23}^2+l_{34}^2-l_{24}^2\right)}{l_{23}l_{34}}}d_1}\right] \tag{6}$$

$$T_k = F_kd_1\sin\theta \tag{7}$$

$$\begin{cases} R_{2x} = \frac{(-A_1\sin\beta + B_1P_{24x})}{P_{24x}\cos\beta + P_{24y}\sin\beta} \\ R_{2y} = \frac{\left(A_1\cos\beta + B_1P_{24y}\right)}{P_{24x}\cos\beta + P_{24y}\sin\beta} \\ A_1 = -(T_{54} + T_{64} + T_1 + T_2) \\ B_1 = -(F_{5x} + F_{6x} + F_{7x})\cos\beta - \\ \quad \left(F_{5y} + F_{6y} + F_{7y}\right)\sin\beta \end{cases} \tag{8}$$

$$\begin{cases} R_{4x} = -(R_{2x} + F_{5x} + F_{6x}) \\ R_{4y} = -\left(R_{2y} + F_{5y} + F_{6y}\right) \end{cases} \tag{9}$$

$$F_\beta = F_{7x}\cos\beta + F_{7y}\sin\beta \tag{10}$$

In the above equations, k denotes the spring stiffness, a denotes the original length of the spring, P_{ijx} and P_{ijy} denote the distance in x and y directions, respectively, R_{ix} and R_{iy} denote the reaction forces of joint i in the x and y directions, respectively, F_{ix} and F_{iy} denote the forces acting on point i in x and y directions, respectively, T_{ij} denotes the torque of the

force acting on point i to point j, T_i denotes the torque acting on point i, and T_k denotes the torque of spring force to point N_3.

Supposing that the counterclockwise direction is positive, T_{53} and T_{63} denote the torque of the gravities of the two links N_2N_3 and N_3N_4 to point N_3, respectively, ΔT denotes the driving torque of the metamorphic revolute joint:

$$\begin{cases} T_{23} = P_{23x}R_{2y} - P_{23y}R_{2x} \\ T_{43} = P_{43x}R_{4y} - P_{43y}R_{4x} \\ T_{53} = P_{53x}m_{23}g \\ T_{63} = P_{63x}m_{43}g \end{cases} \tag{11}$$

$$\Delta T = T_{23} - T_{43} + T_{53} - T_{63} \tag{12}$$

In working configuration II, the AAG RRRP degenerates into the RRR group. The force analysis of the corresponding equivalent Assur group RRR is shown in Figure 6, where points N_5 and N_6 are the centroids of the links N_2N_3 and N_3N_4, respectively. Given that forces F_5, F_6 and torques T_1, T_2 act on the links N_2N_3 and N_3N_4, respectively, solve the reaction force of each revolute joint and the driving torque and constraint torque of the metamorphic revolute joint. According to the above conditions, the reaction force of each revolute joint and the driving torque and constraint torque of the metamorphic revolute joint are solved.

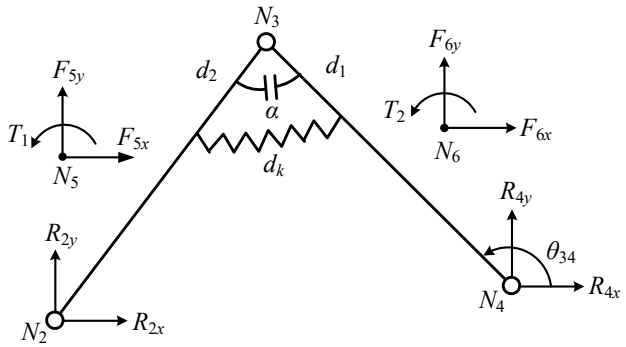

Figure 6. Force diagram of RRR group degraded by RRRP group.

Modularized force analysis procedures are as follows:

$$\begin{cases} R_{4x} = \frac{(A_2P_{43x} - B_2P_{42x})}{P_{43x}P_{42y} - P_{43y}P_{42x}} \\ R_{4y} = \frac{(A_2P_{43y} - B_2P_{42x})}{P_{43x}P_{42y} - P_{43y}P_{42x}} \\ A_2 = -(T_{51} + T_{61} + T_1 + T_2) \\ B_2 = -(T_{63} + T_2 + T_k) \end{cases} \tag{13}$$

$$\begin{cases} R_{2x} = -(R_{4x} + F_{5x} + F_{6x}) \\ R_{2y} = -(R_{4y} + F_{5y} + F_{6y}) \end{cases} \tag{14}$$

$$\begin{cases} R_{3x} = -(R_{4x} + F_{6x} + F_{kx}) \\ R_{3y} = -\left(R_{4y} + F_{6y} + F_{ky}\right) \\ F_{kx} = F_k\cos(\theta_{34} + \theta - \pi) \\ F_{ky} = F_k\sin(\theta_{34} + \theta - \pi) \end{cases} \tag{15}$$

In the above equations, F_{kx} and F_{ky} denote the components of the spring force in x and y directions, respectively. The calculation method of the variables d_k, θ, F_k, T_k, ΔT and the meaning of the other variables can refer to the force analysis in working configuration I above.

3.2. Structure Design of Metamorphic Revolute Joint According to Constraint Parameters Calculated in Modularized Force Analysis

When the metamorphic revolute joint keeps static in a working configuration, the angle of its two links must be constrained, neither increasing nor decreasing. The common way to keep static is to use spring force constraints and/or geometric constraints in the structure design of metamorphic joints. In previous studies, metamorphic joints are often drawn in kinematic diagrams without structure design. For practical application, a simple and practical structure of the metamorphic revolute joint is designed in the paper as shown in Figure 7a,b, and the physical prototype is shown in Figure 7c.

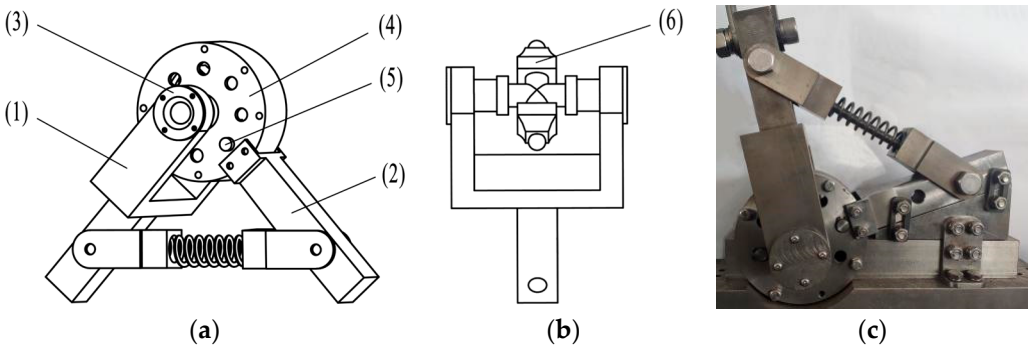

Figure 7. Structure of metamorphic revolute joint.

The link (1), the end cover (3) and the component (6) are connected as a united one, as shown in Figure 7b. The link (2) and the component (4) are connected as a united one by bolts. The balls at both ends of the component (6) can move along the grooves which are located on the internal surface of the component (4), so that the two links (1) and (2) can rotate relative to each other. As shown in Figure 7a, the pin (5) serves as an actual geometric constraint, and the angle of the metamorphic revolute joint cannot increase after the component (6) contacts the pin (5). The spring is compressed with a preload and installs on the links. When the driving torque of the metamorphic revolute joint is large enough to overcome the force of the compressed spring, link (2) rotates clockwise relative to link (1) due to the release of both geometrical constraint and spring force constraint.

At the limiting position, geometric constraints of the metamorphic revolute joints theoretically provide infinite constrained force to ensure that the angle cannot increase. At the same time, if the metamorphic revolute joint plans to keep static in a working configuration, the constraint torque provided by the spring force from preload should be greater than the maximum value of driving torque during the entire process of configuration keeping to limit the reduction of the angle between links (1) and (2), that is, as follows:

$$F_k \geq \frac{\Delta T}{d_1 \sin\theta} \tag{16}$$

F_k is the spring force from preload, d_1 and θ are the corresponding structural dimensions as shown in Figure 5. Furthermore, we can design the structural parameters of spring by using the range of spring preload calculated by Equation (16).

4. Probabilistic Evaluation Model for the Configuration Transformation Ability of Constrained Metamorphic Mechanisms

In general, the probabilistic evaluation procedure for the configuration transformation ability of constrained metamorphic mechanisms is shown in Figure 8, and the detailed steps to perform the probabilistic evaluation will be introduced in the following sections.

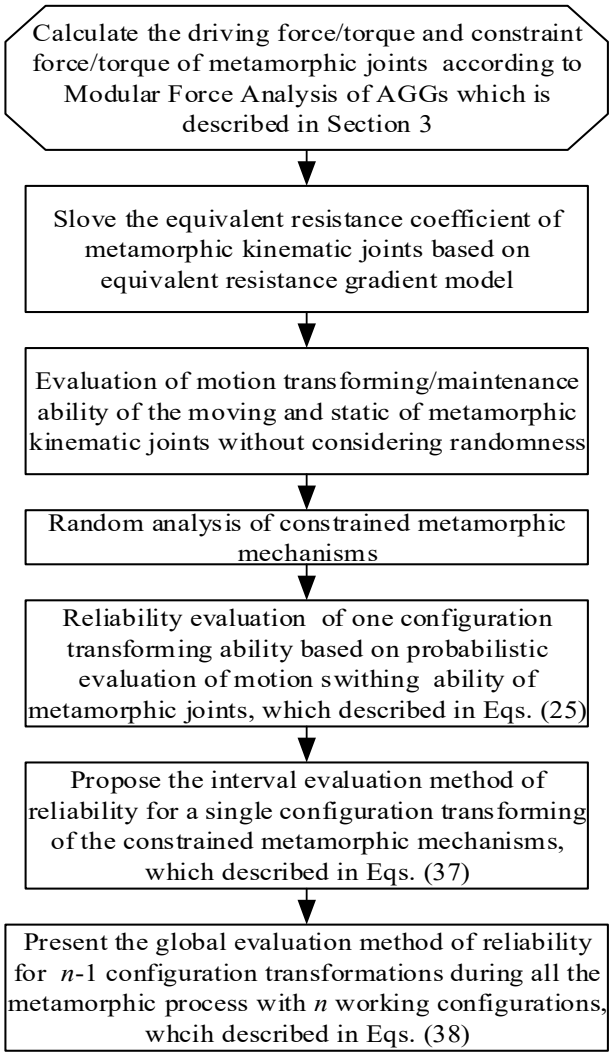

Figure 8. Flowchart for probabilistic evaluation procedure of configuration transformation ability of constrained metamorphic mechanisms.

4.1. Evaluation of Configuration Transformation Ability Based on Equivalent Resistance Gradient Model

In order to enable the constrained metamorphic mechanism to accurately complete the configuration transformation and realize the desired movements, the types and constraint architectures of metamorphic joints should be determined. Moreover, the constraint forces of the corresponding metamorphic joints should be calculated. Therefore, the equivalent resistance gradient model is established in ref. [7]. First, a dimensionless coefficient $f_e(\theta_i)$ is defined:

$$f_{em}(\theta_i) = \left|\frac{F_c(\theta_i)}{F_{\min}}\right| = \left|\frac{T_c(\theta_i)}{T_{\min}}\right| \tag{17}$$

$$f_{es}(\theta_i) = \left|\frac{F_c(\theta_i)}{F_{\max}}\right| = \left|\frac{T_c(\theta_i)}{T_{\max}}\right| \tag{18}$$

$f_{em}(\theta_i)$ is the equivalent resistance coefficient of moving metamorphic joint in the working stages, $f_{es}(\theta_i)$ is the equivalent resistance coefficient of static metamorphic joint in the working stages. $F_{\min}$ and $T_{\min}$ are the minimum driving force and torque acted on moving metamorphic joint in the corresponding working stages, respectively. $F_{\max}$ and $T_{\max}$ are the maximum driving force and torque acted on static metamorphic joint in the corresponding working stages, respectively.

The moving sequences of metamorphic joints should be proportional to the equivalent resistant forces coefficient according to the law of minimum resistance of kinematics. Therefore, the equivalent resistance gradient of the metamorphic joints in the working stages of constrained metamorphic process should be as follows:

$$f_{es}(\theta_i) \geq 1 \text{ and } f_{em}(\theta_i) \leq 1 \tag{19}$$

Taking the constrained metamorphic mechanism shown in Figure 1 as an example, the force analysis method of the RRRP augmented Assur group can be referred to in Section 3.1. According to Equations (17)–(19), the equivalent resistance coefficients of metamorphic joints R_3 and P_7 must meet the following conditions in the two configurations:

In working configuration I, the metamorphic revolute joint R_3 should always keep static, and the metamorphic prismatic joint P_7 should always keep moving to ensure the desired working sequence. The driving torque of joint R_3 is provided by ΔT in Equation (12), and the constraint torque is provided by the spring force constraint and geometric constraint together. When $\Delta T < 0$, the angle of the metamorphic revolute joint R_3 tends to increase, but remains unchanged due to geometric constraint. When $\Delta T > 0$, the angle of joint R_3 tends to decrease and the spring is compressed. In order to still keep joint R_3 static during working configuration I, the constraint torque provided by the spring should be always greater than the driving torque:

$$f_{e3} = \frac{F_k d_1 \sin\theta}{\Delta T} \geq 1 \tag{20}$$

The beginning of working configuration II is regarded as the moment of configuration transformation. At that moment, the metamorphic prismatic joint P_7 begins to switch from moving to static because of geometric constraint, and the metamorphic revolute joint R_3 begins to change from static to moving. Since the geometric constraint force is theoretically infinite, it is obvious that the probability of the metamorphic prismatic joint P_7 to finish the configuration transformation is nearly 100%. In order to complete the switch from static to moving of metamorphic revolute joint R_3 accurately at the moment of configuration transformation, the driving torque at that moment should be greater than the constraint torque of the spring force:

$$f'_{e3} = \frac{F_k d_1 \sin\theta}{\Delta T} < 1 \tag{21}$$

In working configuration II, the metamorphic prismatic joint P_7 should always keep static, and the metamorphic revolute joint R_3 should always keep moving to ensure the desired working sequence. Since the slider is under geometric constraints, the constraint force is theoretically infinite, so the slider can never move to the right. At the same time, in order to ensure that the slider cannot move to the left, the component of the reaction force on the slider along the moving direction should be always to the right and greater than the leftward component of the external force along the moving direction of the slider:

$$f_{e7} = \frac{R_{4x}\cos\beta + R_{4y}\sin\beta}{|F_\beta|} \geq 1 \tag{22}$$

The calculation formulas of R_{4x} and R_{4y} are shown in Equation (13), F_β is the component of the external force on the slider along the moving direction, as shown in Figure 5, as shown in Equation (10), and β is the angle between the moving direction and the horizontal axis.

4.2. Random Analysis of Configuration Transformation of Constrained Metamorphic Mechanisms

In practical application, there are a lot of uncertain factors, such as the uncertainties of link dimensions, clearances of joints and fit errors caused by manufacturing tolerances, masses and moment of inertia, spring stiffness, size and installation errors in metamorphic joints with spring force constraints, the driving errors of actuators, time-varying perfor-

mance degradation typically represented by the increase in clearances of joints caused by wear et al. The factors can lead to the fact that the driving force and constrained force of any metamorphic joints in metamorphic mechanisms produced according to the same blueprint are not determined values, but random variables with some certain distributions. For the reason above, the actual equivalent resistance coefficients of the metamorphic joints are also random variables. Figure 8 shows the ideal equivalent resistance coefficient curves of the metamorphic joints R_3 and P_7 of the mechanism shown in Figure 1 and two of the actual curves randomly selected when errors are considered in configuration II. From Figure 9a, it can be seen that the actual equivalent resistance coefficients f_3 and f_7 fluctuate randomly in their envelope of confidence region. According to the equivalent resistance gradient model, the equivalent resistance coefficient $f_e = 1$ is the boundary value between moving and static of the metamorphic joints. When it is near the moment of configuration transformation, the equivalent resistance coefficient of metamorphic joint of force constrained is closer to 1 (Figure 9a). Therefore, the fluctuation of its value is more likely to cause the failure of the kinematic status transformation of metamorphic joints and then result in the failure of configuration transformation of constrained metamorphic mechanisms. Obviously, the analysis above also confirms the conclusion that the failure of configuration transformation is the most likely failure model of constrained metamorphic mechanism from the perspective of force analysis. Figure 9b shows the equivalent resistance coefficient curves of two metamorphic joints with spring force constraints. Due to the random fluctuation of the two equivalent resistance coefficients at the moment θ_{CT}, the probability of successful configuration transformation of constrained metamorphic mechanisms with the spring force constraints is usually lower than that of the mechanism with a geometric constraint and a spring force constraint, as shown in Figure 8. Obviously, compared with the deterministic model, it is of more practical engineering significance than how to define and solve the probability of successful configuration transformation.

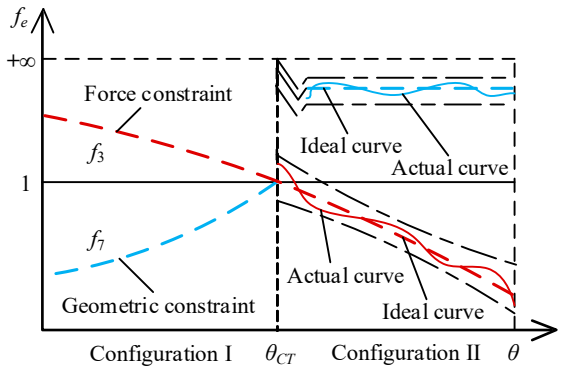

(**a**) Actual equivalent resistance coefficients in working configuration II

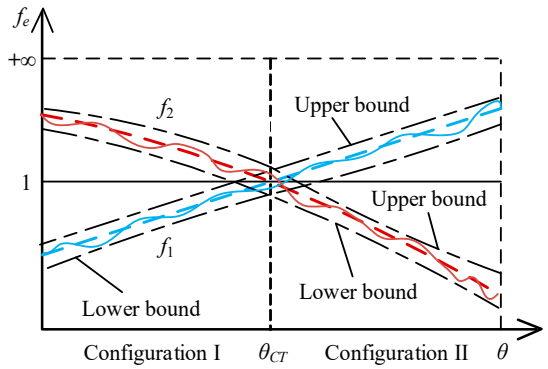

(**b**) Actual equivalent resistance coefficients in working configurations I and II

Figure 9. Actual equivalent resistance coefficients of metamorphic joints.

4.3. Reliability Evaluation Model of Configuration Transformation Ability

Given the randomness of the driving force F and the resistance F_c of a metamorphic joint k, when the kinematic status of the metamorphic joint changes from static to moving at the moment of configuration transformation, the reliability of kinematic status transformation is as follows:

$$\begin{aligned} R_k &= P(f_e < 1) = P(F > F_c) \\ &= \int_{-\infty}^{\infty} f_s(x_s) \left[\int_{-\infty}^{x_s} f_1(x_1) \mathrm{d}x_1 \right] \mathrm{d}x_s \end{aligned} \tag{23}$$

When the metamorphic joint switches from moving to static at the moment of configuration transformation, the reliability is as follows:

$$\begin{aligned} R_k &= P(f_e > 1) = P(F < F_c) \\ &= \int_{-\infty}^{\infty} f_s(x_s) \left[\int_{x_s}^{\infty} f_1(x_1) \mathrm{d}x_1 \right] \mathrm{d}x_s \end{aligned} \tag{24}$$

$f_s(x_s)$ is the probability density function of the driving force, and $f_1(x_1)$ is the probability density function of the resistance force.

Obviously, the configuration transformation of the metamorphic mechanism is mainly realized by switching the motion state of metamorphic joints. Therefore, the probability of the successful transformation moment of the constrained metamorphic mechanism with n working configurations at a single configuration transformation is defined as the product of the probabilities R_k of the successful kinematic status transformations of n metamorphic joints. The joints participate in configuration transformation of constrained metamorphic mechanisms:

$$R_c = \prod_{i=1}^{n} R_{ki} = P(f_{e1}(\theta_{CT}) < 1) \prod_{i=2}^{n} P(f_{ei}(\theta_{CT}) > 1) \tag{25}$$

θ_{CT} is the position angle of driving link at the moment of configuration transformation.

According to the equivalent resistance gradient curves shown in Figures 8 and 9, the equivalent resistance coefficient is close to 1 at the adjacent moments of the configuration transformation. At the moment, the fluctuation in equivalent resistance coefficient is more likely to cause the undesired working sequence. Therefore, it is necessary to give the interval reliability calculation model of the configuration transformation.

Planar metamorphic joints are divided into metamorphic revolute joints and metamorphic prismatic joints, and both of them exit in augmented Assur group RRRP, as shown in Figure 3. Therefore, taking the constrained metamorphic mechanism (Figure 1) with the RRRP augmented Assur group as an example, the interval reliability calculation model of the configuration transformation is established, which can provide reference to analyze the configuration transformation reliability of constrained metamorphic mechanisms containing other augmented Assur groups. Moreover, the force analysis method of the RRRP augmented Assur group can be referred to in Section 3.1. Some factors need to be considered, such as the uncertainties in the link dimensions, masses, angular velocity and angular displacement of driving link, spring stiffness, installation position of spring and constrained angular of geometric constraint. Meanwhile, it is assumed that all the uncertainty parameters are random variables, and each of them is expressed by an independent and normal, i.e., Gaussian distribution.

As described in Section 4.1, whether the mechanism shown in Figure 1 can work well in working configuration I is mainly determined by whether the metamorphic revolute joint R_3 can keep static all the time.

Take Equations (8), (9), (11) into Equation (12), respectively, to calculate the driving torque of metamorphic revolute joint R_3:

$$\begin{aligned} \Delta T_1 = \quad & T_{23} - T_{43} + T_{53} - T_{63} = \\ & P_{23x}R_{2y} - P_{23y}R_{2x} - P_{43x}R_{4y} + \\ & P_{43y}R_{4x} + P_{53x}m_{23}g - P_{63x}m_{34}g = \\ & f(l_{12}, l_{23}, l_{34}, \alpha, m_{23}, m_{34}, m_{slider}, \omega_1, \theta_1) \end{aligned} \tag{26}$$

Bring Equations (4), (6) into Equation (7), respectively, to calculate the resistance torque of metamorphic revolute joint R_3:

$$\begin{aligned} T_k \quad & = F_k d_1 \sin\theta \\ & = k(a - d_k) d_1 \sin\theta \\ & = f(k, d_1, d_2, \alpha) \end{aligned} \tag{27}$$

Therefore, the limit state function of the ability of the metamorphic revolute joint R_3 to keep static in working configuration I is expressed as follows:

$$Z_1 = T_k - \Delta T_1 \tag{28}$$

At the moment of configuration transformation, the metamorphic prismatic joint P_7 begins to switch from moving to static, and the metamorphic revolute joint R_3 changes from static to moving. Since the geometric constraint force is theoretically infinite, the probability of joint P_7 to complete the configuration transformation is regarded to be nearly 1. Therefore, whether the mechanism shown in Figure 1 can complete configuration transformation at the moment is mainly determined by whether joint R_3 can switch form static to moving accurately.

Take Equations (11), (13), (14) into Equation (12), respectively, to obtain the driving torque of joint R_3 at the moment of configuration transformation:

$$\begin{aligned} \Delta T_{CT} = \quad & T_{23} - T_{43} + T_{53} - T_{63} = \\ & P_{23x}R_{2y} - P_{23y}R_{2x} - P_{43x}R_{4y} + \\ & P_{43y}R_{4x} + P_{53x}m_{23}g - P_{63x}m_{34}g = \\ & f(l_{12}, l_{23}, l_{34}, k, d_1, d_2, \alpha, m_{23}, m_{34}, \omega_1, \theta_1) \end{aligned} \tag{29}$$

The spring is not compressed at the moment of configuration transformation. Consequently, the consistent torque of joint R_3 keeps constant as Equation (27). Therefore, the limit state function of the kinematic status transformation ability of joint R_3 at the moment of configuration transformation is expressed as Equation (30) similarly:

$$Z_{CT} = \Delta T_{CT} - T_k \tag{30}$$

In order to ensure the desired working sequence in working configuration II, joint P_7 should always keep static. To keep joint P_7 static, the slider requires sufficient driving force. In other words, the resultant force of the reaction force and the external force along the guide path is always to the right.

The component of the reaction force on the slider along the moving direction is as follows:

$$\begin{aligned} R_\beta \quad & = R_{4x}\cos\beta + R_{4y}\sin\beta \\ & = f(l_{12}, l_{23}, l_{34}, k, d_1, d_2, m_{23}, m_{34}, \omega_1, \theta_1) \end{aligned} \tag{31}$$

The calculation formula of R_{4x} and R_{4y} is shown in Equation (13).

The component along the moving direction of the external force F_β acted on the slider is shown in Equation (10).

In most cases, the direction of the reaction force on the slider is to the right, and the direction of the external force is to the left. Therefore, the limit state function of the ability of joint P_7 to keep static in working configuration II can be expressed as follows:

$$Z_2 = R_\beta - F_\beta \tag{32}$$

By applying the method of First-Order Second Moment, the first-order Taylor expressions of the limit state function of the above three working stages are expanded, and the error models of the limit state function are established. Taking the moment of configuration transformation as an example, the mean μ_{T_1} and variance $\sigma^2_{T_1}$ are calculated, respectively:

$$\mu_{Z_{CT}} = f\left(\mu_{l_{12}}, \mu_{l_{23}}, \mu_{l_{34}}, \mu_k, \mu_{d_1}, \mu_{d_2}, \mu_\alpha, \mu_{m_{23}}, \mu_{m_{34}}, \mu_{\omega_1}, \mu_{\theta_1}\right) \tag{33}$$

$$\begin{aligned} \sigma^2_{Z_{CT}} = \; & \left(\frac{\partial f}{\partial l_{12}}\right)^2 \sigma^2_{l_{12}} + \left(\frac{\partial f}{\partial l_{23}}\right)^2 \sigma^2_{l_{23}} + \left(\frac{\partial f}{\partial l_{34}}\right)^2 \sigma^2_{l_{34}} + \\ & \left(\frac{\partial f}{\partial \alpha}\right)^2 \sigma^2_k + \left(\frac{\partial f}{\partial m_{23}}\right)^2 \sigma^2_{d_1} + \left(\frac{\partial f}{\partial m_{34}}\right)^2 \sigma^2_{d_2} + \\ & \left(\frac{\partial f}{\partial \alpha}\right)^2 \sigma^2_\alpha + \left(\frac{\partial f}{\partial m_{23}}\right)^2 \sigma^2_{m_{23}} + \left(\frac{\partial f}{\partial m_{34}}\right)^2 \sigma^2_{m_{34}} + \\ & \left(\frac{\partial f}{\partial \omega_1}\right)^2 \sigma^2_{\omega_1} + \left(\frac{\partial f}{\partial \theta_1}\right)^2 \sigma^2_{\theta_1} \end{aligned} \tag{34}$$

Since the limit state functions of the three working stages of the constrained metamorphic mechanism (Figure 1) are known, and both the driving torque and the resistance torque accord with normal distribution, by applying the stress strength interference model, the reliability of configuration transformation/keeping ability of constrained metamorphic mechanisms is as follows:

$$R = P(Z > 0) = \int_0^\infty f(Z)\mathrm{d}Z = \int_0^\infty \frac{1}{\sqrt{2\pi}\sigma_Z} \exp\left[-\frac{1}{2}\left(\frac{Z - \mu_Z}{\sigma_Z}\right)^2\right]\mathrm{d}Z \tag{35}$$

Equation (36) is obtained by converting Equation (35) into standard normal distribution and sets $z = \frac{Z-\mu_Z}{\sigma_Z}$

$$R = \int_{z_0}^\infty \frac{1}{\sqrt{2\pi}} \exp\left[-\frac{1}{2}z^2\right]\mathrm{d}z = 1 - \Phi(z_0) = \Phi(\beta) \tag{36}$$

$$z_0 = -\frac{\mu_Z}{\sigma_Z};\ \beta = \frac{\mu_Z}{\sigma_Z}$$

$f(Z)$ is the limit state function whose mathematical expressions are Equations (28), (30) and (32) corresponding to configuration I, configuration II and the moment of configuration transformation, respectively. Take the configuration transformation moment for example, the actual expression of the limit state function $f(Z_{CT})$ could be solved by Equations (27), (29) and (30). Moreover, the partial derivative $\frac{\partial f}{\partial x_i}$ for each input parameter x_i (i = 1, 2, 3, . . ., n) can be solved. Therefore, μ_Z and σ_Z could be obtained. Due to page limitations, we will not go into details about the actual expression of $f(Z_{CT})$, μ_Z and σ_Z.

The constrained metamorphic mechanism is more likely to produce an undesired working sequence at the adjacent moment of configuration transformation. Therefore, in working configurations I and II of the equivalent resistance gradient curve, a and b adjacent moments of configuration transformation whose equivalent resistance coefficients are close to 1 are respectively selected to calculate the reliability of the corresponding moments. Referring to the reliability calculation of the series system, multiply the reliabilities of (a + b) adjacent moments with the reliability R_c of the successful configuration transformation at the moment of configuration transformation. The interval evaluation method of reliability

R_j for a single configuration transformation of the constrained metamorphic mechanism with two working configurations is as follows:

$$R_j = \prod_{i=1}^{a} R_{1i} R_c \prod_{i=1}^{b} R_{2i} \tag{37}$$

R_{1i} is the reliability of the ith adjacent moment near configuration transformation in working configuration I, and R_{2i} is the reliability of the ith adjacent moment near configuration transformation in working configuration II. Generally, the metamorphic mechanism with n working configurations needs to complete $n-1$ configuration transformations, so the global reliability of successful configuration transformation during the entire metamorphic process of the constrained metamorphic mechanism with n working configurations is as follows:

$$R_n = \prod_{j=1}^{n-1} R_j \tag{38}$$

R_j is the reliability of a single configuration transformation, and n is the number of working configurations.

5. Reliability Optimization Design Method Oriented to the Stability of Configuration Transformation

Reliability optimization design is an important part of reliability design, which means that under certain constraints, the best design scheme is given in accordance with the corresponding objective requirements. The general approach is to establish a mathematical model of design variables, objective functions and constraints for engineering problems and then use intelligent optimization algorithms to calculate the optimal results. The general mathematical optimization model can be described as follows [49,50]:

$$\begin{cases} \min & f(d, X, Y) \\ s.t. & \Pr\{g_i(d, X, Y) \geq 0\} \geq [R_i] \qquad i = 1, 2, \cdots n_g \\ & d^l < d < d^u \\ & \mu_X^l < \mu_X < \mu_X^u \end{cases} \tag{39}$$

$f(d, X, Y)$ is the objective function; d is the deterministic design variable; X is the random design variable vector, which is controlled by the designer during the design process; Y is the uncertainty design parameter, which is not controlled by the designer during the design process; $\Pr\{\bullet\}$ is the probability of no failure; $g_i(d, X, Y)$ is the performance function related to the failure mode; n_g is the number of performance functions; d^l and d^u are the lower and upper limits of d, μ_X is the mean value of random design variable X, μ_X^l and μ_X^u are the lower and upper limits of μ_X.

Compared with the traditional mechanical structure, metamorphic structure has the function of configuration transformation, and the failure of configuration transformation is a common failure form of metamorphic structure. Compared with the reliability optimization results of motion accuracy, the reliability optimization results oriented to configuration transformation ability can meet the needs of practical work of metamorphic structures.

5.1. Determination of Optimization Design Parameters Based on Reliability Sensitivity Analysis

The discreteness of random variables of each structural parameter has different influence on the reliability of the configuration transformation of the metamorphic mechanism. If the variation in some structural parameter tolerance has a great influence on the reliability, it should be strictly controlled. Otherwise, the restrictions on them can be relaxed to reduce processing costs. Therefore, before the reliability optimization design of the configuration transformation ability of the metamorphic mechanism is carried out, the variance sensitivity of each structural parameter needs to be determined. Moreover, the random parameters whose tolerance values need to be strictly controlled should be determined, and the tolerance values should be selected as the optimization design variables.

The variance sensitivity [51] of the configuration transformation reliability of the constrained metamorphic mechanism to the structural parameter vector $X = [x_1, x_2, \cdots, x_n]^T$ is as follows:

$$\frac{\partial R}{\partial Var(X)} = \frac{\partial R}{\partial \beta}\frac{\partial \beta}{\partial \sigma_Z}\frac{\partial \sigma_Z}{\partial Var(X)} \tag{40}$$

It can be seen from Equations (35) and (36):

$$\frac{\partial R}{\partial \beta} = \varphi(\beta),\ \frac{\partial \beta}{\partial \sigma_Z} = -\frac{\mu_Z}{\sigma_Z^2},\ \frac{\partial \sigma_Z}{\partial Var(X)} = \frac{1}{2\sigma_z}\left[\frac{\partial \overline{z}}{\partial X} \otimes \frac{\partial \overline{z}}{\partial X}\right]$$

Z is the limit state function. At the moment of working configuration I, configuration transformation and working configuration II, its expressions are Equations (28), (30) and (32), respectively. $\varphi(\bullet)$ is the probability density function of the standard normal distribution. $Var(X)$ represents the variance of the structural parameter vector. The symbol $\otimes$ represents the Kronecker product, which is defined as $(A)_{p\times q} \otimes (B)_{s\times t} = \left(a_{ij}B\right)_{ps\times qt}$.

Due to the inconsistency of units among the structural parameters that affect the reliability of the configuration transformation of the metamorphic mechanism, the reliability sensitivity of different parameters cannot be compared. Therefore, it is necessary to conduct dimensionless processing for reliability sensitivity [52]. After the dimensionless processing, the reliability to each variance sensitivity of structural parameters is as follows:

$$s_{x_i} = \frac{\partial R}{\partial Var(X)}\frac{\sigma_{x_i}^2}{R} \tag{41}$$

In order to better analyze the influence of the tolerance of each parameter on reliability, the variance sensitivity value is normalized to obtain the variance sensitivity coefficient S_{x_i} of each parameter:

$$S_{x_i} = \left|\frac{s_{x_i}}{\sum s_{x_i}}\right| \tag{42}$$

According to the calculation result of variance sensitivity coefficient of each parameter, tolerance of the parameter with higher sensitivity is taken as the optimization design variable.

5.2. Objective Function

The objective of optimization design is usually the lowest cost, lightest weight and highest stiffness. The objective function of the paper adopts a tolerance–cost model which can be constructed in many ways, such as exponential model, power exponential model, linear model and composite model. The commonly used power exponential model is selected by the paper, and the objective function established is as follows:

$$\cos t(x) = \sum_{i=1}^{n} k_i (c_i)^{-\alpha_i} \tag{43}$$

α_i is the processing cost characteristic index [53] formulated according to the mechanical manufacturing process theory, generally α_i = 0.7~1 (α_i = 0.7 is used in the paper). k_i is the cost weight coefficient of the tolerance items of each parameter, and it is generally impossible to give an exact value in the optimization design stage. In the paper, combined with the analysis results of variance sensitivity, the variance sensitivity coefficient of each parameter is used as its cost weighting coefficient; n represents the number of optimization design variables.

Due to the different dimensions of each parameter in the optimization design, there is a large order of magnitude difference between each parameter. Therefore, the optimization result can be affected. In order to deal with the dimensionless calculation of the relative

cost and optimize the variation coefficient c_i of each parameter by the optimization model in the paper, $cost(x)$ is a dimensionless parameter.

5.3. Constraint Condition

(1) Reliability constraints

The objective of the optimization design in the paper is to make the constrained metamorphic mechanism meet the given reliability index requirements of configuration transformation. The constraint condition is as follows:

$$R_n \geq [R_n] \tag{44}$$

$[R_n]$ is the allowable value of the preset reliability of configuration transformation.

(2) Single tolerance boundary condition

In the constraint conditions, the ranges of the coefficients of variation c_i are respectively constrained. The constraint condition is as follows:

$$c_i \leq [c_i] \tag{45}$$

$[c_i]$ (i = 1,2,. . .n) is the allowable value of the coefficient of variation of the corresponding parameter.

5.4. Reliability Optimization Design Based on Improved Genetic Algorithm

With the development of optimization theory and computer technology, many new optimization algorithms have been produced and widely used. The different results of reliability optimization are often due to the different optimization algorithms. In the paper, an improved genetic algorithm combining genetic algorithm with nonlinear programming algorithm (fmincon function) is adopted.

Compared with other optimization algorithms, the improved genetic algorithm has obvious advantages in many aspects. Compared with the ant colony algorithm (ACO), the improved genetic algorithm emphasizes more effective global optimization ability and adaptability in solution space search. Compared with particle swarm optimization (PSO), the improved genetic algorithm pays more attention to the local optimization ability of genetic operation while maintaining population diversity. Compared with the Markov Chain Monte Carlo method (MCMC), it avoids the long-term dependence of Markov Chain through population evolution mechanism and is more suitable for efficient large-scale optimization problem solving.

Genetic algorithm simulates the process of biological evolution in nature. First, an initial population is generated, in which each individual represents a possible solution. Then, the population is gradually optimized through operations such as selection, crossover and mutation to achieve the final stop condition.

Due to the limitation of population number and iteration times, genetic algorithm has strong global search ability but weak local search ability. In addition, the algorithm also has some defects, such as "premature", which leads it to attain the sub-optimal solution of the problem sometimes but not the optimal solution. The nonlinear programming algorithm is also a mathematical optimization method, which aims to find the best solution to complex problems by solving the maximum or minimum value of the objective function. Nonlinear programming algorithm relies on the gradient information of objective function to guide the adjustment of decision variables in order to achieve the best solution. Nonlinear programming algorithm has strong local search ability but weak global search ability. Therefore, the two algorithms can be combined to form an improved genetic algorithm.

The tuning process of the improved genetic algorithm is shown in Figure 10.

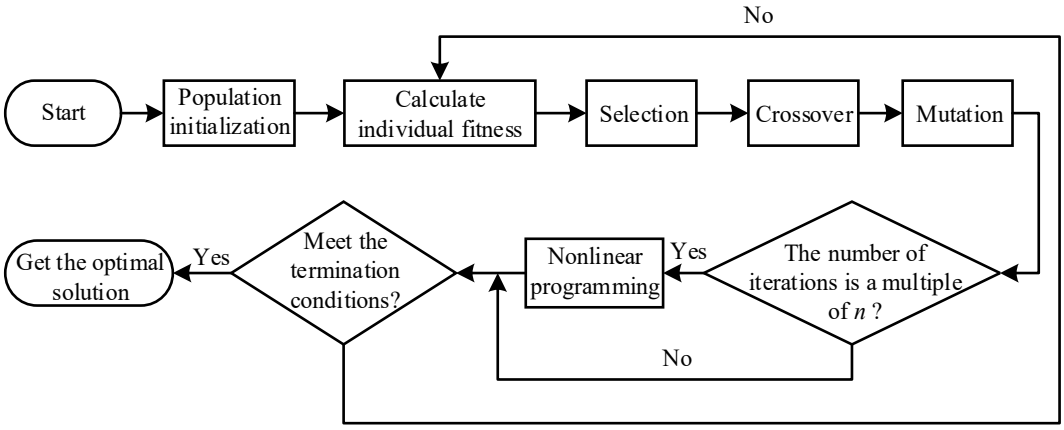

Figure 10. The tuning process of the improved genetic algorithm.

The tuning process of the improved genetic algorithm is interpreted in detail as follows:

(1) Population initialization.

The paper adopts the real number coding method, and each chromosome is a real number vector.

(2) Individual fitness.

The fitness function is the standard to evaluate the quality of individuals in a population. It is generally obtained by transforming the objective function. In the paper, the objective function of the optimization model is taken as the fitness function.

(3) Selection.

Selection is based on the sorting results of individuals according to fitness values to eliminate poor individuals and retain excellent individuals to pass on to the next generation. The paper uses the roulette wheel selection, the probability of individual selection p_i is as follows:

$$p_i = \frac{f_i}{\sum_{j=1}^{N} f_j} \tag{46}$$

f_i is the individual fitness value; N is the total number of individuals in the population.

(4) Crossover.

Crossover is to simulate the sexual reproduction process of natural organisms. It exchanges some genes between two jointed chromosomes according to the crossover probability to form two new individuals. Since individuals are encoded by real numbers, the real number crossover method is used in the paper to simulate the uniform crossover of binary representation. The crossover operation method of the kth chromosome a_k and the lth chromosome a_l at position j is as follows:

$$\begin{cases} a_{kj} = a_{kj}(1-b) + a_{lj}b \\ a_{lj} = a_{lj}(1-b) + a_{kj}b \end{cases} \tag{47}$$

b is a random number in the interval [0,1].

(5) Mutation.

Mutation refers to the replacement of certain gene values in the individual code string with other gene values according to the mutation probability to form a new individual. The paper uses Gaussian mutation operator, which means replacing the original gene value with a random number conforming to the normal distribution of mean μ and variance σ2 during mutation operation. Assuming that there are 12 random numbers $r_i(i = 1, 2, \cdots, 12)$ uniformly distributed in the range of [0,1], a random number conforming to the normal distribution $N(\mu, \sigma^2)$ can be obtained by the following equation:

$$Q = \mu + \sigma\left(\sum_{i=1}^{12} r_i - 6\right) \tag{48}$$

When Gaussian mutation operation is performed from $X = x_1 x_2 \cdots x_k \cdots x_l$ to $X = x_1 x_2 \cdots x'_k \cdots x_l$, the value range of gene value at mutation point x'_k is $\left[U^k_{\min}, U^k_{\max}\right]$, and we assume as follows:

$$\begin{cases} \mu = \frac{U^k_{\max}+U^k_{\min}}{2} \\ \sigma = \frac{U^k_{\max}+U^k_{\min}}{6} \end{cases} \tag{49}$$

The new gene value x'_k can be determined by the following equation:

$$x'_k = \frac{U^k_{\max} + U^k_{\min}}{2} + \frac{U^k_{max} + U^k_{\min}}{6}\left(\sum_{i=1}^{12} r_i - 6\right) \tag{50}$$

(6) Nonlinear programming.

The MATLAB R2021b (version number: 9.11) optimization toolbox contains the fmincon function that can be directly called on to solve nonlinear programming problems. The function starts from an estimated value to search the minimum value of the nonlinear multivariate function under the constraint condition.

The MATLAB program code of improved genetic algorithm for reliability optimization of configuration transformation ability of metamorphic mechanisms is shown in the Supplementary Materials.

6. Calculation Example of the Paper Folding Metamorphic Mechanism

6.1. Type Synthesis of the Paper Folding Mechanism

The folding process of cardboard is shown in Figure 11. There are two steps: in the first step, from Figure 11a to Figure 11b, cardboard 1 and cardboard 2 keep relatively static, and they are folded into 90° along the crease between 2 and 3. In the second step, from Figure 11b to Figure 11c, cardboard 2 and cardboard 3 keep relatively static and they are folded into 90° along the crease between 1 and 2.

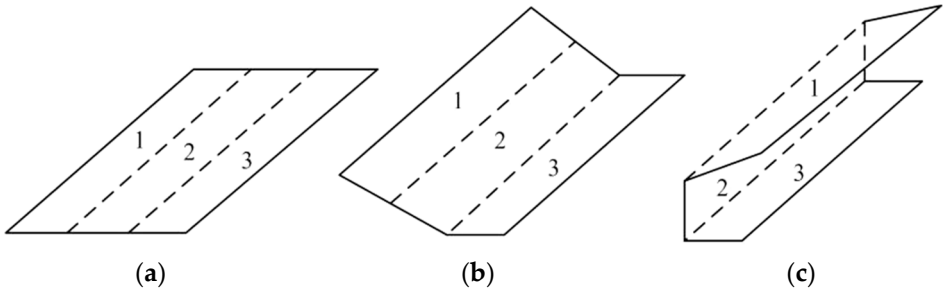

Figure 11. The folding process of cardboard.

For the first step of folding paper in the horizontal direction, it could be completed by using a crank–slider mechanism. For the second step in the vertical direction, it could be completed by using a crank–rocker mechanism. Based on the structural design of the metamorphic revolute joint in Section 3.2, the kinematic diagram of a 2-DOF constrained metamorphic mechanism with two working configurations which could perform the whole folding process is shown in Figure 12. The constrained metamorphic mechanism is divided into three parts: the driving link, RRR Assur group and RRRP augmented Assur group. The RRRP group could switch between the crank–slider mechanism and the crank–rocker mechanism. The ahead RRR group reduces the maximum compression of the spring in the metamorphic revolute joint E. The other spring connected to the slider makes the speed

and acceleration change relatively stable during the movement of the slider and weakens the shock and vibration [38].

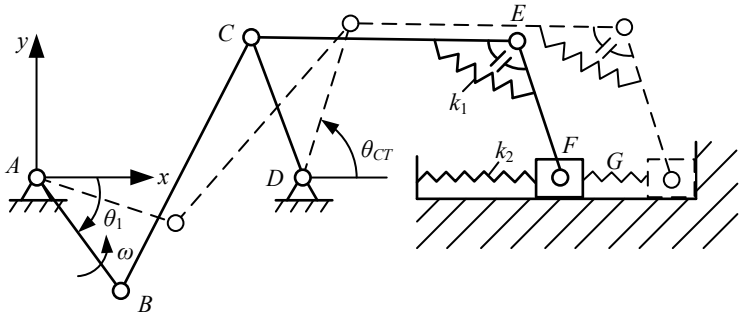

(**a**) Working configuration I

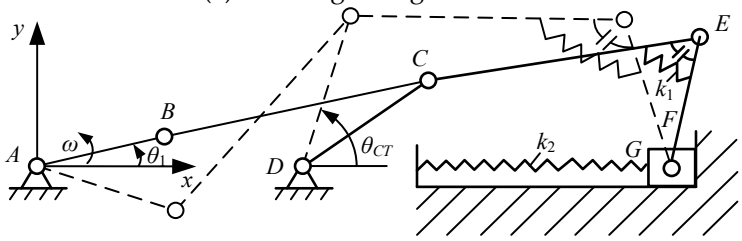

(**b**) Working configuration II

Figure 12. Working stage of the paper folding metamorphic mechanism.

The structural parameters and tolerances produced in the manufacturing process of the paper folding mechanism are shown in Table 1, and the variation ranges of some kinematic parameters are shown in Table 2. In the table, k_1, k_2, a, b are the stiffness and original length of spring 1 and spring 2, d_1 and d_2 are the distances between the installation positions of spring 1 on link EF and link CE and the point E, as shown in Figure 5. Moreover, α is the geometric constraint angle of the metamorphic revolute joint E (the maximum angle of $\angle CEF$), and $\Delta\theta_1$ is the input angle error of the driving link. Finally, It is assumed that all the parameters in Table 1 follow normal distribution, and the value of mean μ_i and standard deviation σ_i of each parameter follow the "3σ" principle.

Table 1. Structural parameters and tolerances of the paper folding mechanism.

Parameter	Value	Parameter	Value	Parameter	Value
l_{AB}/mm	180 ± 0.125	l_{BC}/mm	360 ± 0.18	l_{CD}/mm	240 ± 0.145
l_{CE}/mm	360 ± 0.18	l_{EF}/mm	210 ± 0.145	l_{AD}/mm	315
maxl_{AF}/mm	870	m_{AB}/kg	N~(1, 0.007)	m_{BC}/kg	N~(1.5, 0.01)
m_{CD}/kg	N~(1, 0.007)	m_{CE}/kg	N~(1.5, 0.01)	m_{EF}/kg	N~(2, 0.013)
m_{slider}/kg	N~(1, 0.007)	J_{AB}/(kg·m^2)	0.0027	J_{BC}/(kg·m^2)	0.0162
J_{CD}/(kg·m^2)	0.0048	J_{CE}/(kg·m^2)	0.0162	J_{EF}/(kg·m^2)	0.00735
a/mm	250	k_1/(N/mm)	N~(10, 0.1)	d_1/mm	N~(100, 0.667)
d_2/mm	N~(120, 0.667)	b/mm	76	k_2/(N/mm)	N~(0.5, 0.01)
ω_1/(rad/s)	N~(2π, 0.01)	α/°	N~(120.3, 0.167)	$\Delta\theta_1$/°	N~(0, 0.067)

Table 2. The variation ranges of some kinematic parameters of the paper folding mechanism.

	Configuration I	Configuration II
Type of mechanism	Crank–slider	Crank–rocker
Driving link angle	−290.2°~−15.2°	−15.2°~69.8°
Angle of joint E	Static (120.3°)	120.3°~72.5°
Position of slider	598.5 mm~870 mm	Static (870 mm)
Angle of rocker	Static (115.9°)	115.9°~88.8°

6.2. Reliability Calculation of the Configuration Transformation Ability of the Paper Folding Mechanism

Based on the theoretical calculation model, the kinematic and force analysis of the paper folding mechanism is calculated by MATLAB, and some results are verified by a simulation software package (ADAMS). The comparisons between the results of two calculation methods are shown in Figures 13–15. It can be seen from Figure 13 that the MATLAB calculation of some key mechanical performance parameters in working configuration I is the same as the ADAMS simulation results, which verifies the correctness of the mathematical model of the kinematic and force analysis of the paper folding mechanism. As can be seen from Figure 14, in the whole working configuration I, the driving torque of the metamorphic joint E is less than the constrained torque provided by the spring. Therefore, the metamorphic joint E is always in a constrained state, and the components CE and EF always remain relatively static. From Figure 15, the calculation results of some key mechanical performance parameters in working configuration II are the same by the two methods. In addition, in the whole working configuration II, due to the reaction force on the slider along the horizontal direction always being to the right and greater than the spring force in the left direction, the driving force on the slider, the reaction force along the horizontal component and the spring force is always to the right. The slider is always constrained due to geometric constraint.

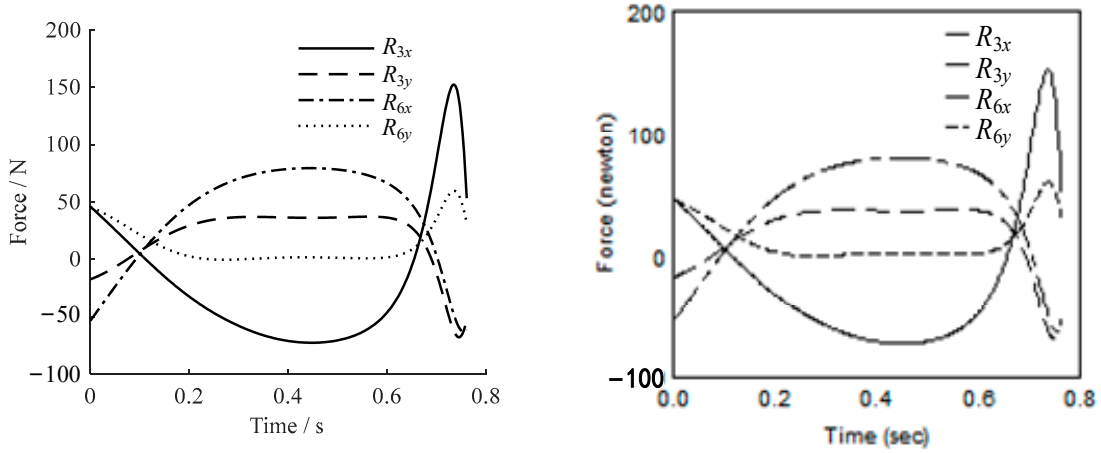

(**a**) MATLAB theoretical calculation (**b**) ADAMS simulation verification

Figure 13. The reaction force of the revolute joint C and the revolute joint F in working configuration I.

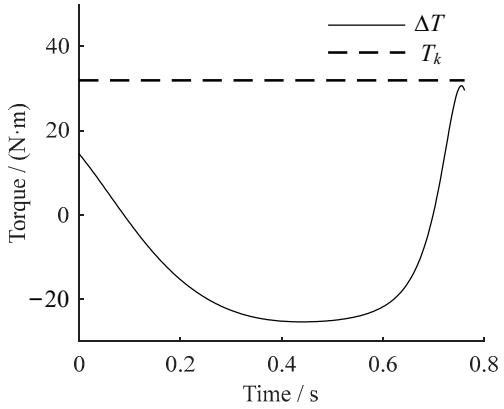

Figure 14. The driving torque ΔT and constrained torque T_k of the metamorphic revolute joint E in working configuration I.

The equivalent resistance coefficients f_E and f_G of metamorphic joints E and G are shown in Figure 16a, and a partial enlarged drawing of f_E near the configuration transformation moment in working configuration I is shown in Figure 16b. Because of the

uncertainty of each parameter in Table 1, the kinematic status transformation of metamorphic revolute joint R_E is likely to be advanced or delayed, which can lead to undesired working sequence. During working configuration II, the equivalent resistance coefficient f_G of joint P_G is positive infinity. However, the reaction force to the right and the spring force to the left are almost similar to each other at the adjacent moment of the configuration transformation according to the force analysis. Therefore, due to the fluctuation in each parameter in Table 1 at these moments which may cause the slider to have a tendency to move to the left and lead to unexpected working sequence of the mechanism, it is necessary to verify their values again.

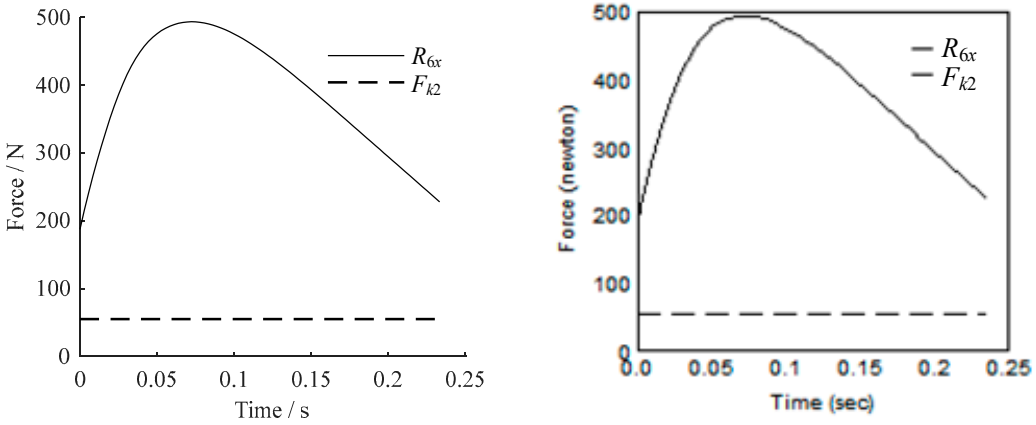

(**a**) MATLAB theoretical calculation (**b**) ADAMS simulation verification

Figure 15. The reaction force R_{6x} and spring force F_{k2} of the slider in working configuration II.

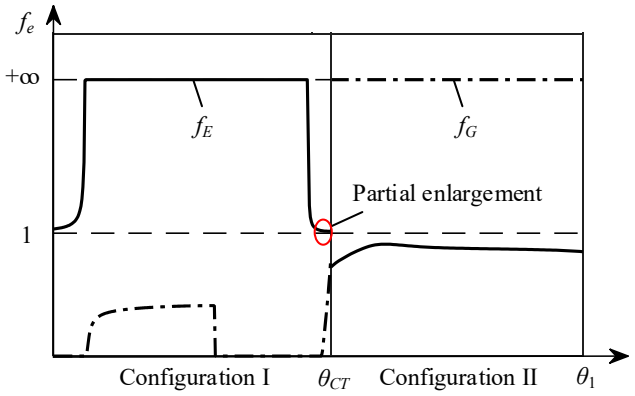

(**a**) Equivalent resistance coefficients of metamorphic joints *E* and *G*

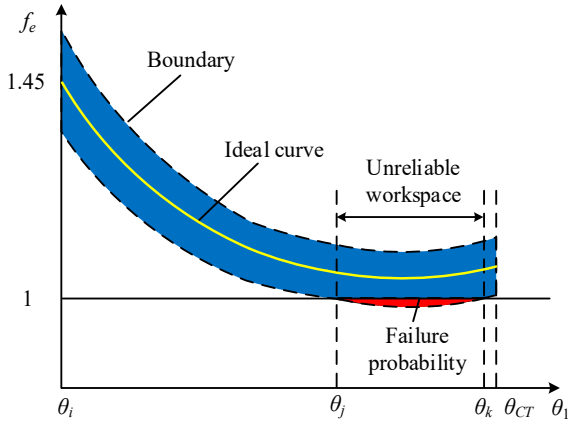

(**b**) Partial enlarged drawing of equivalent resistance coefficient

Figure 16. Equivalent resistance coefficients of the paper folding mechanism.

Based on the probabilistic evaluation model of configuration transformation ability described in Section 4.3, the reliabilities at the moment of configuration transformation and the adjacent moments in working configurations I and II are respectively calculated. Then, the interval reliability of the configuration transformation ability is obtained by multiplying them. When calculating the reliability of the adjacent moment, the reliability is calculated by taking an adjacent moment every 1° from the adjacent moment to the moment far away from the configuration transformation until the value of the reliability is 1. The results of reliability theory calculation and Monte Carlo simulation (MCS) are shown in Table 3 during working configuration I, the moment of the configuration transformation, and working configuration II.

Table 3. The results of reliability theory calculation and Monte Carlo simulation.

Configuration	Angle	μ_Z	σ_Z	β	Reliability	MCS
Conf. I	−21°	2.5817	0.5194	4.9705	1	1
Conf. I	−20°	1.7918	0.5256	3.4088	0.9997	0.9996
Conf. I	−19°	1.3314	0.5337	2.4947	0.9937	0.9633
Conf. I	−18°	1.2474	0.5440	2.2930	0.9891	0.9886
Conf. I	−17°	1.5846	0.5570	2.8449	0.9978	0.9981
Conf. I	−16°	2.3832	0.5729	4.1599	1	1
Transformation moment	−15.2°	42.1336	1.0606	39.7262	1	1
Conf. II	−15°	132.4779	3.8848	34.1016	1	1

According to Equation (38), the interval reliability of configuration transformation ability of the paper folding mechanism is as follows:

$$R_g = R_{11}R_{12}\cdots R_{16}R_cR_{21} = 0.9804$$

6.3. The Optimization Design of Reliability for Configuration Transformation of the Paper Folding Mechanism

The sensitivity calculation model includes the position angle parameter of the driving link. According to the reliability calculation result of the paper folding mechanism, the reliability is the lowest when the position angle of the driving link is −18°. The moment is taken as an example to calculate the variance sensitivity coefficient of each structural parameter. The parameters of the paper folding mechanism are taken into Equations (40)–(42), and the calculation results are shown in Table 4.

Table 4. Variance sensitivity coefficient of each structural parameter of paper folding mechanism.

Parameter	Sensitivity Coefficient	Parameter	Sensitivity Coefficient	Parameter	Sensitivity Coefficient
l_{AB}	0.0075	l_{BC}	0.0065	l_{CD}	0.0030
l_{CE}	0.0003	l_{EF}	0.0003	k_1	0.3449
k_2	0.1904	d_1	0.1149	d_2	0.2019
α	0.0937	m_{CE}	0.0142	m_{EF}	0.0001
m_{slider}	0.0067	ω_1	0.0155	θ_1	0.0002

In order to more intuitively reflect the size relationship of variance sensitivity coefficient of each parameter, the histogram of variance sensitivity coefficient is drawn, as shown in Figure 17.

As can be seen from Figure 17, the variances of the five parameters k_1, k_2, d_1, d_2, and α have a greater impact on the reliability, and the variance of other parameters has a negligible impact on the reliability. In the reliability optimization design, the tolerances of these five parameters are taken as design variables, and the tolerances of other parameters are taken as given values, so that the paper folding mechanism can meet the reliability requirements under the condition of considering economy.

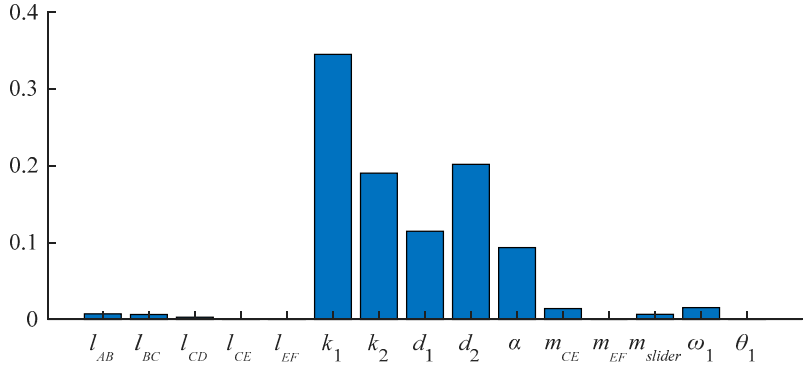

Figure 17. Variance sensitivity coefficient of each parameter of paper folding mechanism.

The optimization model of the paper folding mechanism is as follows:

$$\begin{cases} \cos t(x) = \sum_{i=1}^{5} k_i(c_i)^{-0.7} \\ s.t. \quad R_n \geq 0.9995 \\ \quad 0.005 \leq c_1 \leq 0.01 \\ \quad 0.01 \leq c_2 \leq 0.02 \\ \quad 0.003 \leq c_3 \leq 0.007 \\ \quad 0.003 \leq c_4 \leq 0.006 \\ \quad 0.007 \leq c_5 \leq 0.014 \end{cases} \tag{51}$$

k_i and c_i are the cost weight coefficient and variation coefficient of optimization design variables, respectively. Since the processing cost increases exponentially with the increase in the reliability requirement of the configuration transformation, the reliability requirement is given as 0.9995, so that the processing cost is controlled as much as possible on the premise of ensuring that the paper folding mechanism has high reliability of repeated operations.

In the paper, the variances of five parameters, k_1, k_2, d_1, d_2, and α, are taken as design variables, and the processing cost is objective function. Under the condition that the reliability of configuration transformation is 0.9995, the improved genetic algorithm is adopted for optimization. In the improved genetic algorithm, the population size is 100, the number of chromosomes is 5, and the maximum number of iterations is 200. The program is programmed with MATLAB to find the optimal solution of tolerance distribution of each parameter of the paper folding mechanism by using the optimization model. Through many groups of calculation results, it is found that the optimal solution can be obtained by iteration for about 25 times (at this time, the processing cost reaches the minimum). In the end, this paper only shows the calculation process of the first 50 iterations. The convergence of the best objective during the optimization process is shown in Figure 18, and the partial enlarged drawing of the optimized equivalent resistance gradient curve of the paper folding mechanism at the adjacent moments of the configuration transforming in working configuration I is shown in Figure 19. In the improved genetic algorithm, the population size is 100, the number of chromosomes is 5, and the number of iterations is 50. The program is programmed with MATLAB to find the optimal solution of tolerance distribution of each parameter of the paper folding mechanism by using the optimization model. The convergence of the best objective during the optimization process is shown in Figure 18, and the partial enlarged drawing of the optimized equivalent resistance gradient curve of the paper folding mechanism at the adjacent moments of the configuration transformation in working configuration I is shown in Figure 19.

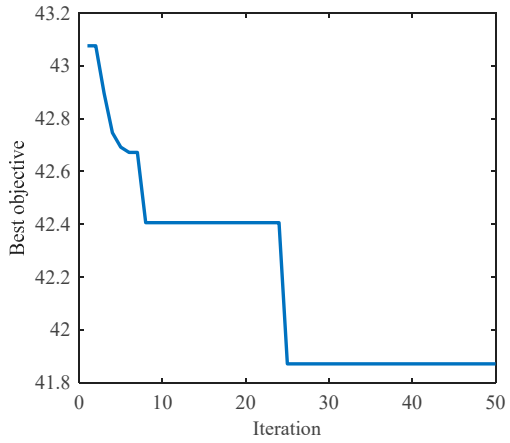

Figure 18. Convergence of the best objective.

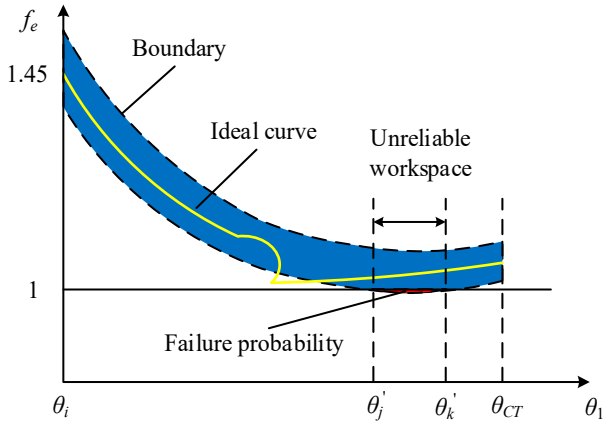

Figure 19. Partial enlarged drawing of equivalent resistance gradient curve after optimization.

The optimization results show that when the iteration reaches 25 times, the optimal fitness value which is the relative cost value obtained by the weight is 41.8704. The tolerances of the five parameters after optimization are shown in Table 5.

Table 5. The tolerances of the five parameters after optimization.

Design Variables	Optimized Result
T_{k_1}	0.348 N/m
T_{k_2}	0.0303 N/m
T_{d_1}	2.58 mm
T_{d_2}	2.736 mm
T_α	1.01°

From the comparison of the partial enlarged drawing of the equivalent resistance coefficient before and after the optimization of the paper folding mechanism (Figures 16b and 19), it can be seen that after optimization, the fluctuation range of the equivalent resistance coefficient at any time is reduced, the unreliable workspace is reduced, and the failure probability of mechanism configuration transformation is reduced (the area of the shaded part in Figure 19 is smaller than that in Figure 16b). As shown in Table 5, three discrete points with low reliability at the configuration transformation moment are selected to compare the changes in equivalent resistance coefficient before and after optimization. Meanwhile, the optimization effect can also be seen in Table 6. The tolerance values of the optimization parameters are taken into the reliability calculation formula of the configuration transformation of the metamorphic mechanism, and the reliability of the configuration

transformation ability of the paper folding mechanism is increased from 0.9804 to 0.9995. Therefore, through the reliability optimization design of the paper folding mechanism, the optimal allocation scheme of each parameter tolerance that meets the given reliability and economic requirements is obtained.

Table 6. Comparison of equivalent resistance coefficient before and after optimization.

Moment	Equivalent Resistance Coefficient f_e	Before Optimization	After Optimization
−17°	Mean value	1.0522	1.0522
	Fluctuation range	14.27%	9.64%
	Failure probability	0.21%	0
−18°	Mean value	1.0406	1.0406
	Fluctuation range	13.84%	9.41%
	Failure probability	1.09%	0.03%
−19°	Mean value	1.0435	1.0435
	Fluctuation range	13.53%	9.30%
	Failure probability	0.63%	0.01%

7. Discussion

(1) Due to the existence of geometric constraints such as the pin (5) shown in Figure 7a and the slider shown in Figure 12b, impacts will be generated inevitably at the moment of configuration transformation for constrained metamorphic mechanisms. The impact force will change the driving torque and constraint torque of the metamorphic joints, which is described in Section 3 Modular Force Analysis of AGGs of this article, it will affect probabilistic evaluation for the configuration transformation ability finally. Due to the small impact force in low-speed situations, in addition, the influence of impact force can be reduced by changing the material, structural form or contact surface curvature of the contact area; the influence of impact force was ignored in this paper. Therefore, the method of probabilistic evaluation and reliability optimization design proposed in this article are limited to the analysis and design of low-speed metamorphic mechanisms.

(2) As shown in Equation (37), The interval evaluation of reliability for a single configuration transformation of the constrained metamorphic mechanism with two working configurations is to multiply the reliabilities $(a + b)$ of adjacent moments near configuration transformation in working configurations I and II with the reliability R_c of the configuration transformation. Obviously, this model refers to the reliability calculation of the series system, which means that failure dependence was ignored at the moment of configuration transformation and the adjacent moments.

8. Conclusions

(1) After reviewing the structure composition principle of the constrained metamorphic mechanism based on the augmented Assur group, the modularized force analysis methods are proposed by taking the driving link, the Assur group and the augmented Assur group containing metamorphic joints as basic units. Based on the definition of the equivalent resistance coefficients of metamorphic joints, the evaluation model of the configuration transformation ability under deterministic conditions is established. Considering the randomness of input errors in the deterministic model, a generalized probabilistic evaluation model for describing the configuration transformation ability of the constrained metamorphic mechanism is established by using the theory of reliability.

(2) Based on the reliability calculation model of the configuration transformation of the constrained metamorphic mechanism, the reliability sensitivity of internal and external parameters of the system is analyzed, and the structural parameter tolerances with high sensitivity are selected as the design variable. Moreover, a reliability opti-

mization model is established with the tolerance–cost model as the objective function and the given reliability of the configuration transformation of the metamorphic mechanism and the tolerance range of each structural parameter as the constraints, so that the optimization scheme satisfies the requirements of reliability and economy at the same time.

(3) Taking the paper folding metamorphic mechanism as an example, the feasibility and effectiveness of the reliability optimization design method are verified. Then, the reliability calculation and reliability optimization design of configuration transformation ability of the paper folding mechanism are completed. The reliability calculation results show that the reliability at the configuration transformation moment is $R = 1$, and the interval reliability of configuration transformation is $R = 0.9804$. The optimization results show that after redistributing the tolerances of key parameters, the fluctuation range of the equivalent resistance coefficient of the paper folding mechanism is reduced, and the interval reliability of the configuration transformation is increased from $R = 0.9804$ to $R = 0.9995$. The optimization results satisfy the given reliability requirements and reduce the cost.

(4) This paper presented an evaluation model of kinematic status switching for metamorphic joints based on equivalent resistance gradient model, a reliability evaluation model of configuration transformation ability and a reliability optimization design method oriented to the stability of configuration transformation for constrained metamorphic mechanisms. Those research works provide the design guidance to obtain the ideal repeated execution ability of configuration transformation, which also have theoretical and practical reference to promote the engineering application for metamorphic mechanisms, reconfigurable mechanisms, and those mechanisms can switch their working configurations. Impact force generated during configuration transformation should be calculated in Modular Force Analysis of AGGs to estimate the dynamics performance of high-speed metamorphic mechanisms. Also, failure dependence of each metamorphic joints was suggested to consider when reliability estimation of constrained metamorphic mechanisms is carried out in future research.

Supplementary Materials: The following supporting information can be downloaded at: https://www.mdpi.com/article/10.3390/app14156524/s1.

Author Contributions: Writing—original draft, Q.Y., H.Z. and B.S.; Writing—review & editing, Y.G. and X.Z. All authors have read and agreed to the published version of the manuscript.

Funding: The work is financially supported by the National Natural Science Foundation of China (Grant No. 51575091), Open Project of Key Laboratory of Lifting Equipment's Safety Technology for State Market Regulation (Grant No. 2023KF002) and the Fundamental Research Funds for the Central Universities (Grant No. N2203010).

Institutional Review Board Statement: Not applicable.

Informed Consent Statement: Not applicable.

Data Availability Statement: The original contributions presented in the study are included in the article and Supplementary Materials, further inquiries can be directed to the corresponding authors.

Conflicts of Interest: The authors declare no conflict of interest.

References

1. Dai, J.S.; Jones, J.R. Mobility in Metamorphic Mechanisms of Foldable/Erectable Kinds. *J. Mech. Des.* **1999**, *121*, 375–382. [CrossRef]
2. Jin, G.G.; Zhang, Q.X.; Dai, J.S.; Li, D.L. Dynamic modeling of metamorphic mechanism. *Chin. J. Mech. Eng.* **2003**, *16*, 94–99. [CrossRef]
3. Dai, J.S.; Ding, X.L.; Zou, H.J. Fundamentals and categorization of metamorphic mechanism. *Chin. J. Mech. Eng.* **2005**, *41*, 7–12. [CrossRef]
4. Guo, Z.H.; Ma, L.Z.; Yang, Q.Z. Topological type analysis of the variable freedom mechanism based on the metamorphic principle. *China Mech. Eng.* **2005**, *16*, 3–5+9.

5. Lan, Z.H.; Du, R. Representation of Topological Changes in Metamorphic Mechanisms with Matrices of the Same Dimension. *J. Mech. Des.* **2008**, *130*, 074501. [CrossRef]
6. Li, S.J.; Dai, J.S. Structure synthesis of single—Driven metamorphic mechanisms based on the augmented Assur groups. *J. Mech. Robot.* **2012**, *4*, 031004. [CrossRef]
7. Li, S.J.; Dai, J.S. *Advances in Reconfigurable Mechanisms and Robotics I*; Springer Press: Tianjin, China, 2012; pp. 53–62.
8. Kanner, O.; Dollar, A. Kinematic Design of an Underactuated Robot Leg for Passive Terrain Adaptability and Stability. *J. Mech. Robot.* **2013**, *5*, 031006. [CrossRef]
9. Coppola, G.; Zhang, D.; Liu, K.F.; Gao, Z. Design of Parallel Mechanisms for Flexible Manufacturing With Reconfigurable Dynamics. *J. Mech. Des.* **2013**, *135*, 071011. [CrossRef]
10. Wang, R.G.; Chen, H.Q.; Li, Y.X.; Zou, Q.M.; Zheng, A.P. Nonlinear dynamic model and simulation of a novel controllable metamorphic palletizing robot mechanism. In Proceedings of the 2014 IFToMM Asian Conference on Mechanism and Machine Science, DYMl-4, Tianjin, China, 9–10 July 2014.
11. Yang, Q.; Wang, H.G.; Li, S.J.; Dai, J.S. Type synthesis of constrained metamorphic mechanisms with structural forms of the metamorphic joints. *J. Mech. Eng.* **2014**, *50*, 1–8. [CrossRef]
12. Li, S.J.; Wang, H.G.; Yang, Q. Constraint Force Analysis of Metamorphic Joints Based on the Augmented Assur Groups. *Chin. J. Mech. Eng.* **2015**, *28*, 747–755. [CrossRef]
13. Wang, Q.C.; Quan, Q.Q.; Deng, Z.Q.; Hou, H.Y. An Underactuated Robotic Arm Based on Differential Gears for Capturing Moving Targets: Analysis and Design. *J. Mech. Robot.* **2016**, *8*, 041012. [CrossRef]
14. Aimedee, F.; Gogu, G.; Dai, J.S.; Bouzgarrou, C.; Bouton, N. Systematization of morphing in reconfigurable mechanisms. *Mech. Mach. Theory* **2016**, *96*, 215–224. [CrossRef]
15. Yan, H.S.; Kuo, C.H. Topological Representations and Characteristics of Variable Kinematic Joints. *J. Mech. Des.* **2006**, *128*, 384–391. [CrossRef]
16. Yan, H.S.; Kang, C.H. Configuration synthesis of mechanisms with variable topologies. *Mech. Mach. Theory* **2009**, *44*, 896–911. [CrossRef]
17. Gan, D.M.; Dai, J.S. Geometry constraint and branch motion evolution of 3-PUP parallel mechanisms with bifurcated motion. *Mech. Mach. Theory* **2013**, *61*, 168–183. [CrossRef]
18. Zhang, K.T.; Dai, J.S.; Fang, Y.F. Geometric constraint and mobility variation of two 3SvPSv metamorphic parallel mechanisms. *J. Mech. Des.* **2013**, *135*, 011001. [CrossRef]
19. Zlatanov, D.S.; Bonev, I.; Gosselin, C. Constraint singularities as configuration space singularities. In *Advances in Robot Kinematics: Theory and Applications*; Springer: Berlin/Heidelberg, Germany, 2002; pp. 183–192.
20. Gan, D.M.; Dai, J.S.; Dias, J.; Seneviratne, L. Unified kinematics and singularity analysis of a metamorphic parallel mechanism with bifurcated motion. *J. Mech. Robot.* **2013**, *5*, 031004. [CrossRef]
21. Tian, H.B.; Ma, H.W.; Ma, K. Method for configuration synthesis of metamorphic mechanisms based on functional analyses. *Mech. Mach. Theory* **2018**, *123*, 27–39. [CrossRef]
22. Qiao, S.L.; Guo, H.W.; Liu, R.Q.; Deng, Z.Q. Self-adaptive grasp process and equilibrium configuration analysis of a 3-DOF UACT robotic finger. *Mech. Mach. Theory* **2019**, *133*, 250–266. [CrossRef]
23. Song, Y.Y.; Chang, B.Y.; Jin, G.G.; Wei, Z.; Li, B.; Zhu, Y.J. Research on Dynamics Modeling and Simulation of Constrained Metamorphic Mechanisms. *Iran. J. Sci. Technol. Trans. Mech. Eng.* **2021**, *45*, 321–336. [CrossRef]
24. Yang, Q.; Hao, G.B.; Li, S.J.; Wang, H.G.; Li, H.Y. Practical Structural Design Approach of Multicon guration Planar Single-Loop Metamorphic Mechanism with a Single Actuator. *Chin. J. Mech. Eng.* **2020**, *33*, 29–43. [CrossRef]
25. Liu, S.L.; Wang, X.D.; Kong, J.Y.; Zeng, T.; Tang, W. Kinematic Reliability Analysis of Planar Metamorphic Mechanism with Multi-source Uncertainties. *J. Mech. Eng.* **2021**, *57*, 64–75.
26. Liao, P.; Lu, J.S. A Calculating Metod of Circle Error Using Genetic Algorithms. *J. Nanjing Univ. Aeronaut. Astronaut.* **1999**, *31*, 393–397.
27. Pan, F.W. Accuracy synthesis of new typed 6 DOF parallel robot based on self-adaptive genetic algorithm. *J. Mach. Des.* **2006**, *26*, 28–31.
28. Pan, F.W.; Lu, J.H.; He, L.L. Analysis of Kinematics of a Novel 6-DOF Parallel Platform Based on Genetic Algorithm. *Mach. Tool Hydraul.* **2009**, *37*, 37–40.
29. Chen, X.L.; Sun, X.Y. Dexterity analysis of a 4-ups-rps parallel mechanism. *Int. J. Adv. Robot. Syst.* **2012**, *9*, 144. [CrossRef]
30. Chen, X.L.; Jiang, D.Y.; Chen, L.L.; Wang, Q. Kinematics Performance Analysis and Optimal Design of Redundant Actuation Parallel Mechanism. *Trans. Chin. Soc. Agric. Mach.* **2016**, *47*, 340–347.
31. Ni, Y.B.; Shao, C.Y.; Zhang, B.; Guo, W.X. Error modeling and tolerance design of a parallel manipulator with full-circle rotation. *Adv. Mech. Eng.* **2016**, *8*, 1687814016649300. [CrossRef]
32. Xiong, Y. Optimal Design of Double-stage Wheel Hub Reducer System based on Fuzzy Theory. *J. Mech. Transm.* **2017**, *41*, 180–187.
33. Kang, X.; Dai, J.S. Theoretical Difficulties and Research Progresses of Mechanism Reconfiguration in Mechanisms—Evolution Connotation, Furcation Principle, Design Synthesis and Application of Metamorphic Mechanisms. *China Mech. Eng.* **2020**, *31*, 57–71.
34. Yu, J.J.; Liu, K.; Kong, X.W. State of the Art of Multi-mode Mechanisms. *J. Mech. Eng.* **2020**, *56*, 14–27.

35. Dai, J.; An, W.; Wang, R.; Li, L. Design and Analysis of a Humanoid Metamorphic Hand Based on Reconfigurable Hooke Joints. *J. Tianjin Univ. (Sci. Technol.)* **2022**, *55*, 221–229.
36. Zhao, F.; Wu, Y.; Yang, X.; Ding, X.; Xu, K.; Guo, S.; Jin, X. Multimode Design and Analysis of an Integrated Leg-Arm Quadruped Robot with Deployable Characteristics. *Chin. J. Mech. Eng.* **2024**, *37*, 59. [CrossRef]
37. Chang, B.; Han, F.; Zhou, Y.; Jin, G. Impact Dynamics of High-speed Metamorphic Mechanism for Comber. *J. Mech. Eng.* **2024**, *60*, 54–65.
38. Li, X.; Mao, X.; Gao, J.; Wang, B. Impact Analysis of the Parameters Variation on the Dynamic Performance of the Constraints Metamorphic Mechanism. *Mach. Des. Manuf.* **2017**, *12*, 90–93.
39. Zhou, H.; Deng, Z.; Geng, T.; He, Y. Dynamics Simulation Analysis on Configuration Change of Metamorphic Lifting Mechanism Based on ADAMS. *J. Liaoning Petrochem. Univ.* **2024**, *60*, 54–65. Available online: https://link.cnki.net/urlid/11.2187.TH.20231009.1140.026 (accessed on 13 June 2024).
40. Cui, Y.; Li, S. The Reliability Analysis Model of Constrained Meta-morphic Mechanisms Configuration Transformation. *Mach. Electron.* **2016**, *34*, 31–34.
41. Li, X.; Gao, J.; Li, J.; Li, S. Effect of parameters variation on random working configurations of constraints metamorphic mechanism. *J. Cent. South Univ. (Sci. Technol.)* **2017**, *48*, 1499–1504.
42. Gao, J.; Li, X.; Li, S. Randomness analysis on configuration switch of parallelogram metamorphic shifting mechanism. *Chin. J. Constr. Mach.* **2023**, *21*, 209–214.
43. Wang, R.; Chen, H.; Dong, Y. Nonlinear Dynamic Reliability Analysis for a Controllable Metamorphic Palletizing Robot. *J. Mech. Eng.* **2023**, *59*, 189–200.
44. Wang, R.; Chen, H.; Dong, Y.; Hea, S. Reliability analysis and optimization of dynamics of metamorphic mechanisms with multiple failure modes. *Appl. Math. Model.* **2023**, *117*, 431–450. [CrossRef]
45. Li, S.J. A Method of Disassembling Assur-Groups for IDENTIFYING and Modelling by Computer. *J. Northeast. Univ.* **1995**, *16*, 198–201.
46. Assur, L. Investigation of plane hinged mechanisms with lower pairs from the point of view of their structure and classification (in Russian): Part I, II. *Bull. Petrograd Polytech. Inst.* **1913**, *20*, 329–386.
47. Huang, P.; Ding, H.F. Structural synthesis of Assur groups with up to 12 links and creation of their classified databases. *Mech. Mach. Theory* **2019**, *145*, 103668. [CrossRef]
48. Simionescu, P.A. Kinematics of the RRR, RRT (Passive) and RRRR, RRRT (Active) Linkage-Mechanism Building Blocks with Applications and Reporting of New Findings. *J. Mech. Robot.* **2019**, *11*, 061006. [CrossRef]
49. Xie, L.Y. Issues and Commentary on Mechanical Reliability Theories, Methods and Models. *J. Mech. Eng.* **2014**, *50*, 27–35. [CrossRef]
50. Shan, S.; Wang, G.G. Reliable design space and complete single-loop reliability-based design optimization. *Reliab. Eng. Syst. Saf.* **2008**, *93*, 1218–1230. [CrossRef]
51. Zhang, Y.M.; Huang, X.Z.; He, X.D.; Song, X.Q. Reliable sensitivity design for kinematics accuracy of planar linkage mechanism. *J. Eng. Des.* **2008**, *2008*, 25–28.
52. Zhang, Y.M.; Zhu, L.S.; Tang, L.; Lu, H. Dynamical Stress Reliability and Sensitivity Analysis of Nonlinear Rotor System with Rigid-flexible Structure. *J. Mech. Eng.* **2011**, *47*, 159–165. [CrossRef]
53. Yan, Z.; Guo, R.L. Precision optimization design of plane mechanism with gap. *Machinery* **2013**, *51*, 42–44.